The scaffolding function of the RLTPR protein explains its essential role for CD28 co-stimulation in mouse and human T cells

Romain Roncagalli,[1]* Margot Cucchetti,[1]* Nicolas Jarmuzynski,[1] Claude Grégoire,[1] Elise Bergot,[1] Stéphane Audebert,[3] Emilie Baudelet,[3] Marisa Goncalves Menoita,[1] Anais Joachim,[1] Stéphane Durand,[1] Miloslav Suchanek,[4] Frédéric Fiore,[2] Lichen Zhang,[1,5] Yinming Liang,[1,5] Luc Camoin,[3] Marie Malissen,[1,2]** and Bernard Malissen[1,2]**

[1]Centre d'Immunologie de Marseille-Luminy, Aix Marseille Université, INSERM, CNRS, 13288 Marseille, France
[2]Centre d'Immunophénomique, Aix Marseille Université, INSERM, CNRS, 13288 Marseille, France
[3]CRCM, Marseille Protéomique, Institut Paoli-Calmettes, Aix Marseille Université, INSERM, CNRS, 13009 Marseille, France
[4]Exbio Praha, Vestec, Czech Republic
[5]School of Laboratory Medicine, Xinxiang Medical University, Xinxiang 453003, China

The RLTPR cytosolic protein, also known as CARMIL2, is essential for CD28 co-stimulation in mice, but its importance in human T cells and mode of action remain elusive. Here, using affinity purification followed by mass spectrometry analysis, we showed that RLTPR acts as a scaffold, bridging CD28 to the CARD11/CARMA1 cytosolic adaptor and to the NF-κB signaling pathway, and identified proteins not found before within the CD28 signaling pathway. We further demonstrated that RLTPR is essential for CD28 co-stimulation in human T cells and that its noncanonical pleckstrin-homology domain, leucine-rich repeat domain, and proline-rich region were mandatory for that task. Although RLTPR is thought to function as an actin-uncapping protein, this property was dispensable for CD28 co-stimulation in both mouse and human. Our findings suggest that the scaffolding role of RLTPR predominates during CD28 co-stimulation and underpins the similar function of RLTPR in human and mouse T cells. Along that line, the lack of functional RLTPR molecules impeded the differentiation toward Th1 and Th17 fates of both human and mouse CD4$^+$ T cells. RLTPR was also expressed in both human and mouse B cells. In the mouse, RLTPR did not play, however, any detectable role in BCR-mediated signaling and T cell-independent B cell responses.

INTRODUCTION

In the two-signal model of T cell activation, the first signal is delivered via the TCR after recognition of antigenic peptides bound to MHC molecules, and the second signal provided by the CD28 co-stimulator after it binds to CD80 or CD86 on APCs. By acting in synergy, the TCR and CD28 trigger the association of the cytosolic adaptor CARMA1 (also known as CARD11) with BCL10 and MALT1 to form the CBM complex (Thome et al., 2010; Jiang and Lin, 2012; Wang et al., 2012). The CBM complex serves as a signaling scaffold permitting the assembly of an active I-κB kinase complex that in turn stimulates the NF-κB signaling pathway.

Using an *N*-ethyl-*N*-nitrosurea-mutagenesis screen, we identified a mutation in the mouse *Rltpr* gene (denoted as *Rltpr*^{bas}) and we demonstrated that its product is essential for co-stimulation via CD28 and as a result critical for the development and homeostasis of regulatory T cells (T reg cells; Liang et al., 2013). *Rltpr* is also known as *Lrrc16c* (*Carmil2*), and in mammals it has two paralogs denoted as *Lrrc16a* (*Carmil1*) and *Lrrc16b* (*Carmil3*; Liang et al., 2009). The three members of the LRRC16 family are large (~1,400 aa) multidomain cytosolic proteins with a high degree of sequence similarity (Liang et al., 2009; Zwolak et al., 2013). They comprise an N-terminal noncanonical pleckstrin homology (PH) domain, a leucine-rich repeat (LRR) domain, a homodimerization domain (HD; as demonstrated in the case of LRRC16A), and an extended C terminus that contains a capping protein (CP) interaction (CPI) motif and a proline-rich region (PRR; Zwolak et al., 2013; Edwards et al., 2014). In their free form, CPs bind tightly to the barbed end of actin filaments and block the addition of actin subunits. After binding to CPI motif, the affinity of CP for actin filaments decreases. Therefore, by uncapping actin filaments,

*R. Roncagalli and M. Cucchetti contributed equally to this paper.

**M. Malissen and B. Malissen contributed equally to this paper.

Correspondence to Bernard Malissen: bernardm@ciml.univ-mrs.fr; or Marie Malissen: malissen@ciml.univ-mrs.fr

Abbreviations used: AP-MS, affinity purification followed by mass spectrometry; CP, capping protein; CPI, CP interaction; cSMAC, central supramolecular activation complex; HD, homodimerization domain; LC-MS/MS, liquid chromatography coupled tandem mass spectrometry; LRR, leucine-rich repeat; OST, One-STrEP-tag; pDC, plasmacytoid DC; PH, pleckstrin homology; PRR, proline-rich region; SEE, staphylococcal enterotoxin E.

The Rockefeller University Press $30.00
J. Exp. Med. 2016 Vol. 213 No. 11 2437–2457
www.jem.org/cgi/doi/10.1084/jem.20160579

the members of the LRRC16 family are thought to enhance actin polymerization and play a role in endocytosis, phagocytosis, and the control of cell shape and movement (Yang et al., 2005; Fujiwara et al., 2010; Hernandez-Valladares et al., 2010; Edwards et al., 2014). The fact that RLTPR went unnoticed until recently is likely a result of its very low abundance (2.6×10^3 copies per T cell; Hukelmann et al., 2016).

Glass-supported planar bilayers containing mobile antigenic peptide–MHC complexes and CD80 molecules allow imaging of the immunological synapse that forms at the T cell–planar bilayer interface. Small TCR and CD28 clusters called microclusters nucleate immediately after T cells attach to the planar bilayer and then, driven by a centripetal flow of F-actin, form a central supramolecular activation complex (cSMAC; Yokosuka and Saito, 2010). The *Rltpr*^{bas} mutation affects neither the generation of TCR and CD28 microclusters nor their translocation to the cSMAC in response to antigen stimulation (Liang et al., 2013). RLTPR and RLTPR^{bas} molecules also form microclusters at the immunological synapse in a CD80-dependent manner, and they co-migrate with CD28 microclusters. Remarkably, the *Rltpr*^{bas} mutation abrogated the ability of CD28-RLTPR microclusters to nucleate the accumulation of CARMA1 at the cSMAC, suggesting that RLTPR is essential for co-stimulation via CD28 in that it couples CD28 to CARMA1.

Here, we combined affinity purification followed by mass spectrometry (AP-MS) analysis and mouse functional genomics to determine the mode of action of RLTPR in T cells. Specifically, we developed mice that bear a genetic tag allowing AP-MS analysis of the RLTPR interactome in primary T cells. We showed that CD28, RLTPR, and CARMA1 physically associate after activation, and we identified proteins not found before within the CD28 signaling pathway. Using CRISPR-Cas9 to edit the genome of human Jurkat leukemic T cells, we demonstrated that RLTPR is also essential for co-stimulation via human CD28 and used this model for structure-function analysis of RLTPR.

RESULTS

Quantitative analysis of RLTPR protein expression in mouse lymphoid and myeloid cells

To quantify the expression of the RLTPR protein, we generated a monoclonal antibody (denoted as EM-53) that recognized residues 1147–1272 of mouse RLTPR and cross-reacted with human RLTPR (see Materials and methods). Intracellular staining of mouse thymocyte subsets with EM-53 showed that RLTPR was expressed at the highest level in both CD25$^+$ double-negative (CD4$^-$CD8$^-$) cells and double-positive (CD4$^+$CD8$^+$) cells and down-regulated in CD4$^+$ and CD8$^+$ single-positive thymocytes (Fig. 1 A). CD28 showed a similar reduction of expression during the double-positive to single-positive thymocyte transition (Fig. 1 A). Among peripheral CD4$^+$ and CD8$^+$ T cells, both naive (CD44^{lo}CD62L^{hi}) and effector memory (CD44^{hi}CD62L^{lo}) T cells expressed substantial levels of RLTPR and CD28 (Fig. 1 B). Likewise, RLTPR and CD28 were coexpressed in T reg cells, γδ T cells, and NKT cells (not depicted).

In the B lymphoid lineage, RLTPR was expressed in B cells (CD45R^{high}CD19$^+$) and plasma cells (CD45R$^-$ CD138$^+$; Fig. 1 C). Given that CD28 is induced at the B cell–plasma cell transition (Delogu et al., 2006), bone marrow plasma cells expressed both CD28 and RLTPR (Fig. 1 C). Mouse NK cells can be organized into a CD11b^{lo}CD27^{hi} → CD11b^{hi}CD27^{hi} → CD11b^{hi}CD27^{lo} maturation sequence that is associated with a progressive acquisition of effector functions (Chiossone et al., 2009). Expression of CD28 and RLTPR was elevated in immature NK cells and diminished upon NK cell maturation (Fig. 1 D). Consistent with transcriptomic data available from the ImmGen project, among conventional DCs, monocytes, monocyte-derived DCs, and macrophages, plasmacytoid DCs (pDCs) were the only ones to express RLTPR, which correlated with the expression of CD28 (Fig. 1 E and not depicted). Therefore, RLTPR is not lymphoid-lineage specific as originally thought, and in most lymphoid (T cells, plasma cells, and NK cells) and myeloid (pDC) cells, its expression was coordinated with that of CD28. However, as illustrated by B cells, RLTPR can be also expressed in the absence of CD28.

Gene-targeted mice suitable for proteomics analysis of RLTPR

To identify the RLTPR interactome by AP-MS, we generated a line of gene-targeted mice expressing a One-STrEP-tag (OST) at the C terminus of endogenous RLTPR (Fig. S1 A). Immunoblots of thymocytes from mice heterozygous for the *Rltpr*^{ost} allele (also known as B6-*Rltpr*^{tm1Mal}; called *Rltpr*^{ost} mice here) showed that addition of the 29-aa-long OST sequence had no effect on RLTPR expression and that the RLTPR-OST bait was efficiently affinity purified with Sepharose beads coupled to Strep-Tactin (Fig. S1 B). Analysis of thymus of *Rltpr*^{ost} mice showed a normal sequence of T cell development and the spleen of *Rltpr*^{ost} mice contained normal numbers of γδ T cells and of CD4$^+$ and CD8$^+$ T cells (Fig. S1, C and D). Stimulation of CD4$^+$ T cells purified from WT and *Rltpr*^{ost} mice with antibody to CD3 (anti-CD3) in the presence or absence of anti-CD28 showed that RLTPR-OST molecules had no detrimental effect on the proliferation and production of IL-2 (Fig. S1, E and F). Therefore, thymocytes and T cells of *Rltpr*^{ost} mice are normal.

Double-positive thymocytes—the major population of cells found in the thymus—contained higher levels of RLTPR than peripheral T cells (Fig. 1, A and B), and thymocytes were thus used to determine the RLTPR interactome. Thymocytes from *Rltpr*^{ost} mice were lysed before or after treatment for 30, 120, 300, and 600 s with the tyrosine-phosphatase inhibitor pervanadate, a surrogate for TCR stimulation (Roncagalli et al., 2014), and the proteins bound to RLTPR-OST were isolated using Strep-Tactin-Sepharose beads. After elution with D-biotin (a ligand that binds to Strep-Tactin with a higher affinity than the OST sequence does), proteins were subjected

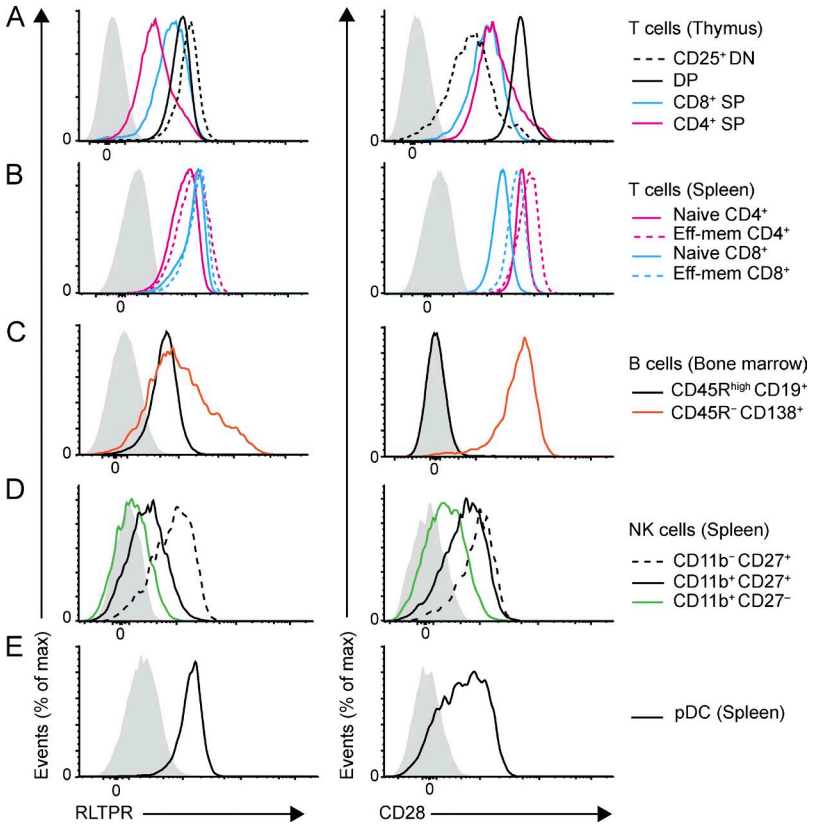

Figure 1. **Quantitative analysis of RLTPR expression in mouse T cells, B cells, NK cells, and pDCs.** (A) Expression of RLTPR (left) and CD28 (right) in double-negative $CD25^+$ thymocytes, double-positive thymocytes, and $CD4^+$ or $CD8^+CD24^-$ single-positive thymocytes, analyzed by flow cytometry using RLTPR- or CD28-specific antibodies. (B) Expression of RLTPR (left) and CD28 (right) in naive and effector memory $CD4^+$ or $CD8^+$ splenic T cells, analyzed by flow cytometry. (C) Expression of RLTPR (left) and CD28 (right) in $CD45R^{high}CD19^+$ B cells and $CD45R^-CD138^+$ plasma cells from the bone marrow, analyzed by flow cytometry. (D) Expression of RLTPR (left) and CD28 (right) in $CD27^+CD11b^-$, $CD27^+CD11b^+$, or $CD27^-CD11b^+$ splenic NK cells, analyzed by flow cytometry. (E) Expression of RLTPR (left) and CD28 (right) in splenic pDCs, analyzed by flow cytometry. pDCs were identified among lineage-negative cells ($CD5^-CD161^-CD19^-$Ly-$6G^-$) on the basis of their $CD317^+CD45R^+SiglecH^+$ phenotype. Results are representative of three experiments involving three animals. Gray shaded curves, negative control staining based on staining of equivalent cell types isolated from RLTPR-deficient (left) or CD28-deficient (right) mice.

to liquid chromatography coupled tandem MS (LC-MS/MS) analysis (see Materials and methods). Three independent biological experiments, each involving five different conditions corresponding to no stimulation and to four time points spanning 600 s after pervanadate stimulation, were analyzed by AP-MS. Technical triplicates were run for each of the five conditions. The reproducibility of the AP-MS process was assessed for each condition of stimulation across biological and technical replicates (Fig. S2). To distinguish truly interacting proteins from nonspecific contaminants, control AP-MS experiments were performed for each time point using WT thymocytes. To determine whether a given detected protein was specifically associated with the RLTPR-OST bait over the course of an experiment, we compared the distribution of log-normalized intensities obtained for *Rltpr*^{ost} and for WT $CD4^+$ T cells. Each comparison yielded a value specifying the enrichment observed in RLTPR-OST thymocytes as compared with WT thymocytes and a corresponding P-value based on a Wilcoxon test (Fig. 2 A). Proteins were selected as specific interacting partners of the considered OST bait when $P < 0.05$ and the corresponding enrichment was greater than threefold (Fig. 2 A and Table S1).

Characterization of the RLTPR interactome

A large spectrum of functional activities was found among the 19 proteins that constitute the RLTPR interactome of thymocytes (Fig. 2 B). They include cytosolic adaptors (CARMA1, FYB [also known as ADAP], GRB2, and GRAP2 [also known as GADS]), the transmembrane adaptor SIT1, two guanine nucleotide exchange factors (VAV1 and DOCK8), a GTPase-activating protein (RASAL3), two receptor protein tyrosine phosphatases (PTPRC [also known as CD45] and PTPRF [also known as LAR]), a cytosolic protein tyrosine phosphatase (PTPN6; also known as SHP1), two transmembrane receptors (CD28 and CD8B), the α- and β-subunits of CP (CAPZA1, CAPZA2, and CAPZB), CNOT1, a subunit of the CCR4–NOT complex, the DEAD-box RNA helicase DDX3X, and the SUGT1 chaperone. CAPZA1, CAPZA2, CAPZB, PTPRC, and SUGT1 associated to RLTPR before activation and remained bound to it after T cell activation (Fig. 2 C). In contrast, all the remaining proteins found in the RLTPR interactome began interacting with RLTPR only after thymocyte activation (Fig. 2 C).

By imaging the immunological synapse, we previously inferred that RLTPR couples CD28 to CARMA1, but due to the extremely low abundance of RLTPR molecules, we failed to validate the existence of such association using conventional biochemistry (Liang et al., 2013). In contrast, the sensitivity of AP-MS analysis readily established that CD28 and CARMA1 associate with RLTPR after thymocyte activation (Fig. 2 C). FYB can be recruited to the CBM complex upon CD3-CD28 stimulation and VAV1 can cooperate with CD28 to contribute to NF-κB activation (Marinari et al., 2002; Srivastava et al., 2010). Consistent with those findings,

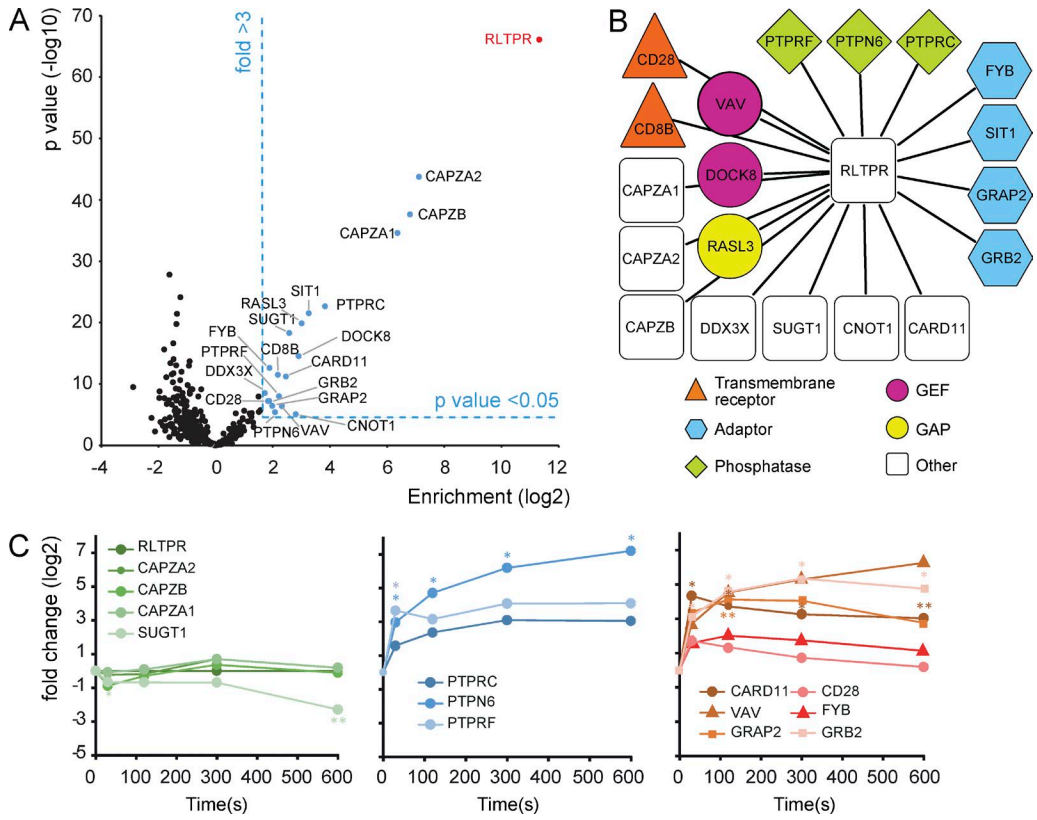

Figure 2. **The RLTPR interactome of thymocytes.** (A) Proteins are classified as RLTPR interactors according to their position in a volcano plot in which the P-value is plotted against the corresponding mean fold-change for RLTPR^{OST} versus WT samples (enrichment). Proteins that displayed enrichment greater than threefold and P < 0.05 were selected as specific partners (shown as blue dots). The RLTPR bait is shown in red, and dashed lines represent thresholds on P-value and enrichment to identify specific RLTPR interactors. (B) Each protein interacting with the RLTPR-OST bait before or after pervanadate stimulation is represented as a node and is linked by an edge to the RLTPR bait. Proteins are identified by their UniProt designations—note that CARD11 corresponds to CARMA1—and are color-coded according to their function or protein family; see key (bottom) and Table S1 for additional information. (C) Kinetics of the binding of proteins to RLTPR. Label-free quantitative analysis of the kinetics of binding of various proteins to RLTPR in thymocytes left unstimulated (0) or stimulated for 30, 120, 300, or 600 s with pervanadate. Kinetics are displayed as fold changes of normalized intensities of association relative to the unstimulated condition. Interacting proteins were clustered by Euclidean distance correlation on the basis of similar binding kinetics. For each protein, binding kinetics was averaged from three independent biological replicates. *, P ≤ 0.05; **, P ≤ 0.01.

both FYB and VAV1 were found in the RLTPR interactome of activated thymocytes (Fig. 2 B). Most of the proteins found in the RLTPR interactome cannot be predicted on the basis of our previous model of RLTPR function (Liang et al., 2013). Among them stood SUGT1, the presence of which can be rationalized in that it has been found to be associated with several cytosolic nucleotide-binding proteins and immune sensors containing LRR domains and is postulated to regulate their stability (Shirasu, 2009; Eastburn et al., 2012). DOCK8, a member of the DOCK180 family of guanine nucleotide exchange factors, is also part of the RLTPR interactome. Several transmembrane receptors and adaptors expressed at the surface of T cells were also found in the RLTPR interactome in addition to the anticipated CD28 receptor. They comprised SIT1, a transmembrane adaptor that contains tyrosine residues that are phosphorylated after TCR stimulation (Horejsí et al., 2004), and the receptor protein tyrosine phosphatases PTPRC and PTPRF. Therefore, the analysis of the RLTPR interactome in T cells demonstrated that RLTPR links CD28 to CARMA1 and unraveled unexpected RLTPR interacting partners.

T cell development and function in RLTPR-deficient mice

To further explore the role of RLTPR in T cell development and function and determine whether the *Rltpr*^{bas} mutation was functionally equivalent to a complete *Rltpr* deficiency, we generated mice deprived of RLTPR by deleting sequences corresponding to exons 1–3 of the *Rltpr* gene (Fig. S3 A). Mice homozygous for this mutation, *Rltpr*$^{-/-}$ (also known as B6-*Rltpr*^{tm2Mal}), were born at the expected Mendelian frequencies and lacked detectable RLTPR protein (Fig. S3 B). Analysis of *Rltpr*$^{-/-}$ mice showed that their thymus and spleen were of normal size (Fig. 3, A and B), and without alteration of CD4, CD8, TCRαβ, and TCRγδ expression

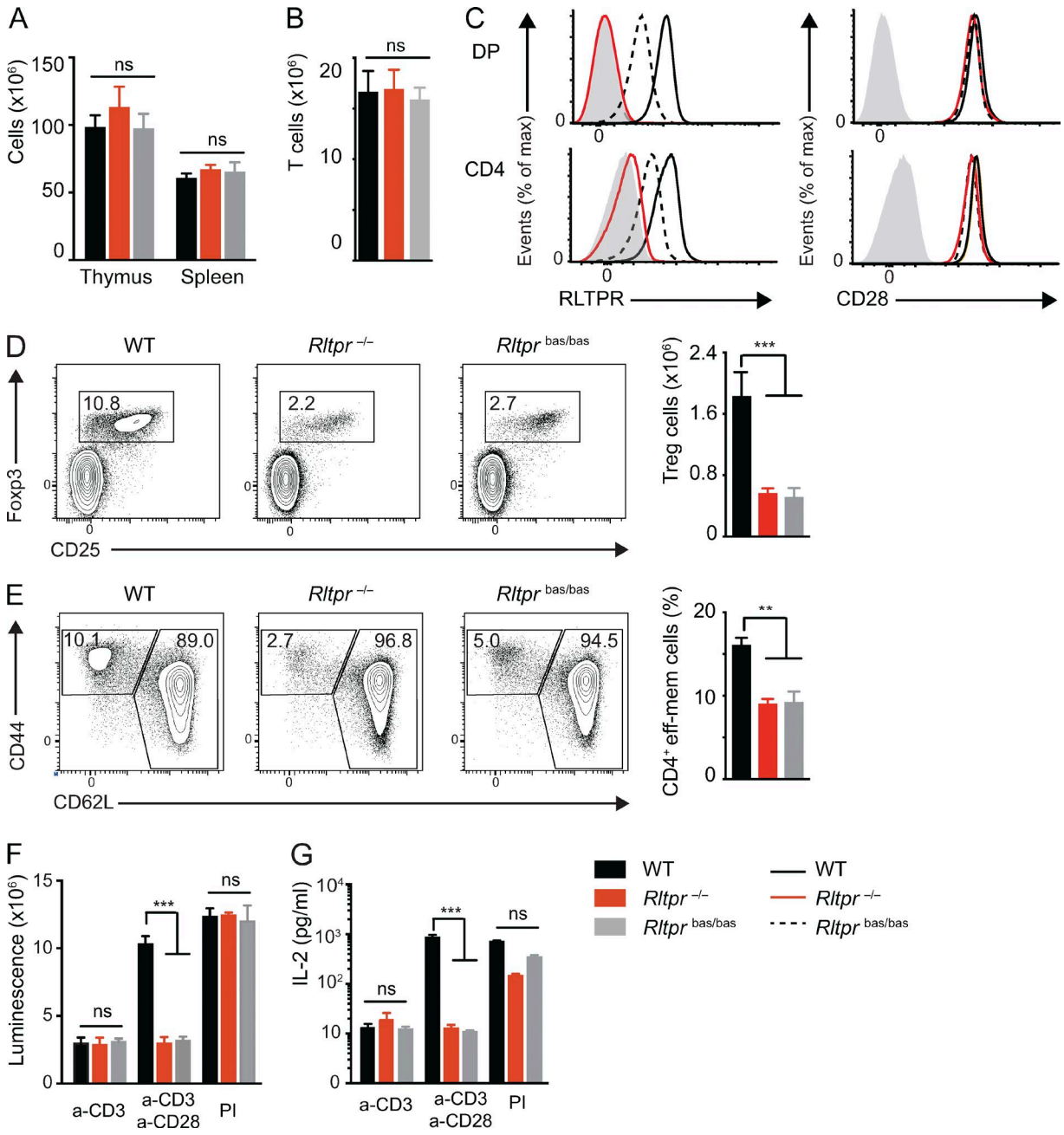

Figure 3. **The *Rltpr*^{bas} mutation phenocopies a *Rltpr*–null mutation.** (A) Cellularity of thymus and spleen of WT, *Rltpr*$^{-/-}$, and *Rltpr*$^{bas/bas}$ mice (key: lower right corner). (B) Quantification of T cells in the spleen of WT, *Rltpr*$^{-/-}$, and *Rltpr*$^{bas/bas}$ mice. (C) Expression of RLTPR (left) and CD28 (right) in double-positive thymocytes (DP) and splenic CD4$^+$ T cells (CD4) from WT, *Rltpr*$^{-/-}$, and *Rltpr*$^{bas/bas}$ mice, analyzed by flow cytometry (key: lower right corner). (D). CD4$^+$ T cells from WT, *Rltpr*$^{-/-}$, and *Rltpr*$^{bas/bas}$ spleens were analyzed for expression of Foxp3 and CD25. Numbers in quadrants indicate percent T reg cells, and quantification of T reg cells is shown on the right. (E) CD4$^+$ T cells from WT, *Rltpr*$^{-/-}$, and *Rltpr*$^{bas/bas}$ spleens were analyzed for expression of CD44 and CD62L. Numbers in quadrants indicate percent naive (CD44^{lo}CD62L^{hi}) and effector memory (CD44^{hi}CD62L^{lo}) CD4$^+$ T cells. Histogram on the right shows percent effector memory CD4$^+$ T cells. (F) ATP content of negatively purified CD4$^+$ T cells from lymph nodes of WT, *Rltpr*$^{-/-}$, and *Rltpr*$^{bas/bas}$ mice, activated for 48 h in vitro with plate-bound anti-CD3 in the presence or absence of soluble anti-CD28 or with PMA and ionomycin (PI). ATP content was assessed using luminescence as a measure of the extent of cell proliferation. (G) IL-2 in supernatants of purified WT, *Rltpr*$^{-/-}$, and *Rltpr*$^{bas/bas}$ CD4$^+$ T cells activated for 48 h as in F. Data are representative of at least three independent experiments, with two to three mice per genotype (D–G; mean and SEM). **, $P \leq 0.01$; ***, $P \leq 0.005$; ns, nonsignificant.

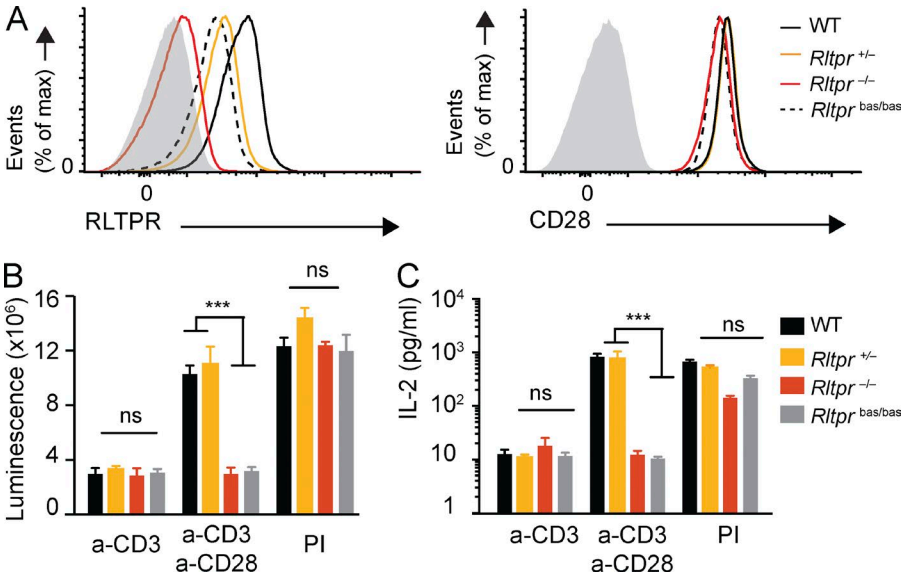

Figure 4. **The lack of CD28 co-stimulation in *Rltpr*$^{bas/bas}$ mice results from the L432P mutation itself and not from the coincidently diminished levels of RLTPR^{bas} protein.** (A) Expression of RLTPR (left) and CD28 (right) in splenic CD4$^+$ T cells from WT, *Rltpr*$^{+/-}$, *Rltpr*$^{-/-}$, and *Rltpr*$^{bas/bas}$ mice, analyzed by flow cytometry. (B) ATP content of negatively purified CD4$^+$ T cells from lymph nodes of WT, *Rltpr*$^{+/-}$, *Rltpr*$^{-/-}$ and *Rltpr*$^{bas/bas}$ mice, activated for 48 h in vitro with plate-bound anti-CD3 in the presence or absence of soluble anti-CD28 or with PMA and ionomycin (PI). ATP content was assessed using luminescence. (C) IL-2 in supernatants of purified WT, *Rltpr*$^{+/-}$, *Rltpr*$^{-/-}$, and *Rltpr*$^{bas/bas}$ CD4$^+$ T cells activated for 48 h as in (B). Data are representative of at least two experiments with three mice per group (B and C; mean and SEM). ***, $P \leq 0.005$; ns, nonsignificant. Gray shaded curves (A), isotype-matched control antibody (negative control).

(Fig. S3, C and D; and not depicted). Developing and mature T cells from WT and *Rltpr*$^{-/-}$ mice expressed identical levels of CD28 at their surface, demonstrating that CD28 expression was not influenced by the presence of RLTPR (Fig. 3 C).

T reg cell development is affected in mice deprived of CD28 or expressing *Rltpr*$^{bas/bas}$ (Fig. 3 D; Liang et al., 2013). Likewise, the spleens of *Rltpr*$^{-/-}$ mice had approximately one third as many Foxp3$^+$ T reg cells as WT spleen had (Fig. 3 D). Both *Rltpr*$^{bas/bas}$ and *Rltpr*$^{-/-}$ mice expressed lower percentages of CD44^{hi}CD62L^{lo} effector memory CD4$^+$ T cells, whereas effector memory CD8$^+$ T cells were not affected (Fig. 3 E and not depicted). Therefore, akin to the situation observed in *Rltpr*$^{bas/bas}$ and *Cd28*$^{-/-}$ mice, the complete absence of RLTPR had a strong impact on T reg cell and effector memory CD4$^+$ T cell development, but was not associated with any impairment of other intrathymic and peripheral T cell subsets.

T cells from *Rltpr*$^{bas/bas}$ and *Rltpr*$^{-/-}$ mice were stimulated with a suboptimal concentration of anti-CD3 in the presence or absence of a fixed concentration of anti-CD28. Analysis of the resulting T cell proliferation and cytokine (IL-2 and IFN-γ) production showed that the RLTPR deficiency prevented CD28 from acting in synergy with the TCR–CD3 complex to the same extent as the *Rltpr*^{bas} mutation did (Fig. 3, F and G; and not depicted). Therefore, the *Rltpr*^{bas} mutation constitutes a functional phenocopy of a complete RLTPR deficiency.

Essential functional role of the LRR domain

Because of the nonconservative L432P substitution identified in the LRR domain encoded by the *Rltpr*^{bas} allele, thymocytes and peripheral T cells of *Rltpr*$^{bas/bas}$ mice contain approximately twofold less RLTPR protein than WT *Rltpr*$^{+/+}$ mice (Fig. 4 A; Liang et al., 2013). Determining whether the lack of CD28 co-stimulation observed in *Rltpr*$^{bas/bas}$ mice resulted from the L432P substitution itself or—more trivially—from the diminished levels of RLTPR^{bas} protein should formally establish whether the LRR domain of RLTPR is critical for its function. For that purpose, we used the *Rltpr*$^{-}$ allele to titrate the number of functional *Rltpr* alleles per T cell. This resulted in a clear gene-dosage effect since CD4$^+$ T cells from *Rltpr*$^{+/-}$ mice expressed approximately twofold less RLTPR protein than WT *Rltpr*$^{+/+}$ mice (Fig. 4 A). The reduced levels of RLTPR found in CD4$^+$ T cells from *Rltpr*$^{+/-}$ mice were without effect on CD28 expression (Fig. 4 A). Analysis of the response of CD4$^+$ T cells from *Rltpr*$^{-/+}$ and *Rltpr*$^{+/+}$ mice to a suboptimal dose of anti-CD3 in the presence or absence of anti-CD28, showed that a twofold reduction in RLTPR had no detectable effect on proliferation and IL-2 production (Fig. 4, B and C). Therefore, given that CD4$^+$ T cells from *Rltpr*$^{bas/bas}$ and *Rltpr*$^{+/-}$ mice contained similar levels of mutant and WT RLTPR molecules, respectively (Fig. 4 A), our results demonstrate that the LRR domain of RLTPR has an essential functional role in CD28 co-stimulation.

RLTPR is essential for the human CD28 signaling pathway

Stimulation of the TCR expressed on the human leukemic T cell line Jurkat with Raji lymphoblastoid B cells presenting the superantigen staphylococcal enterotoxin E (SEE) triggers IL-2 production. Blocking the interaction of CD80 and CD86 on Raji cells with CD28 on Jurkat cells by adding a CTLA4-Ig recombinant fusion protein prevents SEE-triggered IL-2 production, demonstrating its dependence on CD28 signaling (Tian et al., 2015). In contrast, SEE-triggered up-regulation of CD69, an activation marker downstream of the Ras–MAPK–ERK signaling pathway, occurs irrespective of CD28 signaling. To examine the role

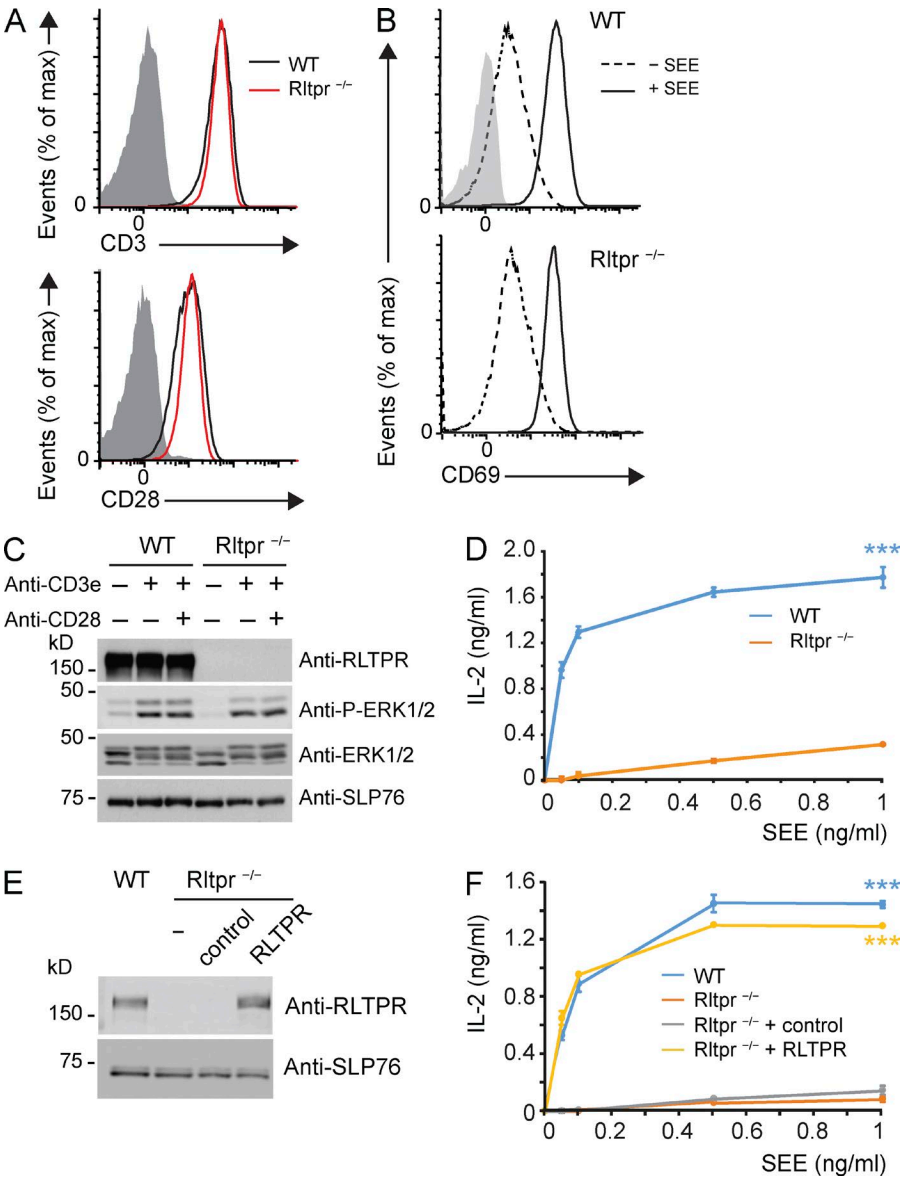

Figure 5. **RLTPR is essential for the function of CD28 in the human T cell line Jurkat.** (A) Expression of CD3 and CD28 on RLTPR-sufficient (WT) and -deficient (*Rltpr*$^{-/-}$) Jurkat cells. (B) RLTPR-sufficient and -deficient Jurkat cells were stimulated with Raji cells in presence (+) or absence (–) of SEE. For each condition, CD69 up-regulation was measured by FACS 24 h after stimulation. (C) RLTPR-sufficient and -deficient Jurkat cells were left untreated (–) of stimulated (+) with anti-CD3 in absence or presence of anti-CD28 for 2 min at 37°C. Equivalent amounts of lysates were analyzed by immunoblot with antibodies specific for RLTPR, ERK1/2, phospho-ERK1/2 (anti–P-ERK1/2), and SLP76 (as a loading control). (D) ELISA analysis of IL-2 production by the specified cells 24 h after stimulation with Raji cells and SEE. (E) Expression of RLTPR using immunoblot of lysates from RLTPR-deficient (*Rltpr*$^{-/-}$) Jurkat cells before (–) and after retroinfection with an empty vector (control) or a vector containing a cDNA coding for RLTPR. WT Jurkat cells were analyzed in parallel, and an anti-SLP76 was used as a loading control. (F) IL-2 production by the cells specified in E 24 h after stimulation with Raji cells and SEE at indicated concentrations. Data are representative of three independent experiments (D and F, mean and SEM are shown; ***, $P \leq 0.005$). Gray shaded curves (A and B, isotype-matched control antibody [negative control]).

of RLTPR in the human CD28 signaling pathway, we generated RLTPR-deficient Jurkat T cells using CRISPR-Cas9 technology (see Materials and methods). The lack of RLTPR did not affect surface expression of CD3 and CD28 (Fig. 5 A), and after stimulation with Raji B cells and SEE, WT and RLTPR-deficient Jurkat cells showed comparable inducible levels of CD69 (Fig. 5 B), and of ERK phosphorylation (Fig. 5 C). In contrast, IL-2 production by SEE-stimulated RLTPR-deficient Jurkat cells was nearly abolished (Fig. 5 D).

To exclude that adventitious recombination events had occurred in RLTPR-deficient Jurkat cells and accounted for their CD28 signaling defect, we infected them with a lentivirus driving the expression of RLTPR. Upon reconstitution, RLTPR-deficient Jurkat cells expressed levels of RLTPR comparable to WT Jurkat cells (Fig. 5 E), and regained their ability to produce IL-2 in response to SEE stimulation (Fig. 5 F). Therefore, RLTPR is essential for the proper function of the CD28 signaling pathway in the human leukemic T cell line Jurkat.

RLTPR exists as a homodimer

LRRC16A, a paralog of RLTPR, contains a central HD that mediates constitutive antiparallel association of two LRRC16A molecules (Zwolak et al., 2013). Fusing a full-length RLTPR protein to a YPET (yellow fluorescent protein for energy transfer) reporter, permitted us to distinguish RLTPR^{OST} and RLTPR^{YPET} molecules in polyacrylamide gels on the basis of their distinct molecular weights (Fig. 6). When lysates of HEK293 cells coexpressing RLTPR^{OST} and RLTPR^{YPET} molecules were subjected to AP with Strep-Actin-Sepharose beads and analyzed by

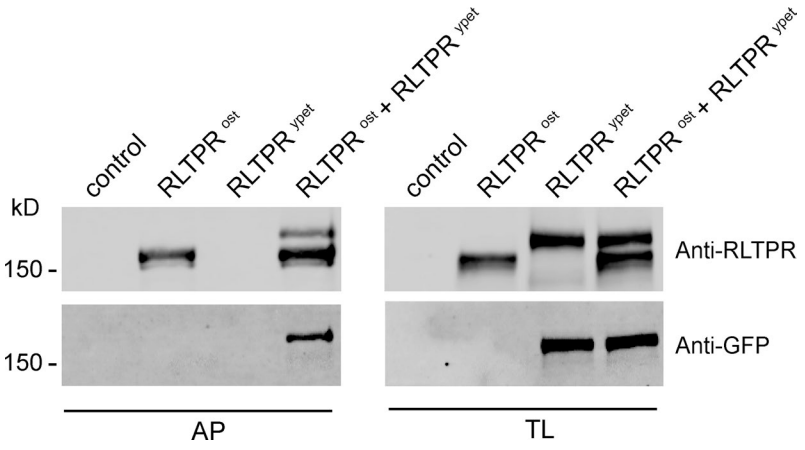

Figure 6. **RLTPR exists as a homodimer.** Equal amount of total lysates from HEK293 cells transfected with an empty vector (control), a vector containing a cDNA coding for $RLTPR^{OST}$, a vector containing a cDNA coding for $RLTPR^{YPET}$, or a 1:1 mixture of the two last vectors were subjected to affinity purification (AP) on Strep-Tactin-Sepharose beads, followed by elution of proteins with D-biotin, and immunoblot analysis with either anti-RLTPR or anti-GFP. Also shown is an immunoblot analysis of equal amount of total lysates (TL) of the same cells probed with the same antibodies. The anti-GFP antibody cross-reacts with YPET. Data are representative of two experiments.

immunoblot with an anti-YPET antibody, $RLTPR^{OST}$ molecules were capable of coprecipitating $RLTPR^{YPET}$ molecules (Fig. 6), demonstrating that, akin to LRRC16A, RLTPR also exists as a constitutive dimer. Considering that the sequence corresponding to the HD found in LRRC16A is poorly conserved in RLTPR and that residues 853–905 of the putative human RLTPR HD are dispensable for dimerization (see Wang et al. in this issue), it remains to determine whether RLTPR dimerization requires sequences distinct from the putative HD or even additional protein partners.

The noncanonical PH domain and the PRR of RLTPR are essential for CD28 co-stimulation in human Jurkat cells

Most previous studies of the function of members of the LRRC16 protein family, including RLTPR, relied on heterologous cellular models and resulted in RLTPR overexpression. The possibility of editing the genome of Jurkat cells with CRISPR-Cas9 permits to express RLTPR mutants in a physiological context and to preserve the stoichiometry of the RLTPR signaling complexes. Sequence alignment suggested that the 158 aa found at the N terminus of human RLTPR code for a noncanonical PH domain similar to the one identified in mouse LRRC16A (Zwolak et al., 2013), whereas the 125 aa found at the C terminus of RLTPR contain a PRR with canonical SH3 domain-binding motifs. After introducing a OST-coding sequence at the C terminus of the two alleles of the *Rltpr* gene found in Jurkat cells, we used the resulting Jurkat cells, denoted as $Rltpr^{ost}$, to derive lines expressing RLTPR molecules deprived of either the noncanonical PH domain ($RLTPR^{DPH}$) or of the PRR ($RLTPR^{DPRR}$; Fig. 7 A). Truncated $RLTPR^{DPH}$ and $RLTPR^{DPRR}$ molecules with the expected molecular weight were expressed at levels comparable to WT RLTPR molecules and were still capable of binding to CP (Fig. 7 B). Jurkat cells expressing $RLTPR^{DPRR}$ molecules showed normal levels of TCR and CD28, whereas normal levels of TCR and slightly reduced levels of CD28 were found on Jurkat cells expressing $RLTPR^{DPH}$ molecules (Fig. 7 C). In response to Raji-SEE, both mutant cell lines showed normal induction of CD69 (Fig. 7 D) and ERK phosphorylation (Fig. 7 B), but failed to produce IL-2 (Fig. 7 E). Therefore, the noncanonical PH domain and the PRR of RLTPR are essential for CD28 co-stimulation in Jurkat cells.

The CPI motif is dispensable for CD28 co-stimulation in Jurkat cells

RLTPR constitutively associates with CP (Fig. 2 B), via its CPI motif and thereby decreases CP affinity for actin filaments (Lanier et al., 2016). To test the importance of the CPI motif for co-stimulation via CD28, we constructed Jurkat T cells expressing RLTPR molecules with a defective CPI motif (denoted as $RLTPR^{DCPI}$ molecules; Fig. 7 A). For that purpose, we changed into alanine a contiguous stretch of 4 aa residues (RPRP) that is conserved and found in the middle of the CPI motif at position 1024–1026 (see Fig. S4 A and Kim et al., 2012 for appropriate sequence alignment and numbering). Changing these residues to alanine has been shown to result in a complete loss of binding to CP in vitro and in fibrosarcoma cells (Lanier et al., 2015). Congruent with those data, immunoblot analysis of $RLTPR^{DCPI}$ molecules isolated from $Rltpr^{dcpi}$ Jurkat cells and probed with anti-CP showed that they have lost their ability to bind CP as compared with WT RLTPR molecules (Fig. 7 F). $Rltpr^{dcpi}$ Jurkat cells showed normal levels of TCR and CD28, and normal induction of CD69 in response to Raji-SEE (not depicted). When stimulated with Raji-SEE, $Rltpr^{dcpi}$ Jurkat cells produced levels of IL-2 nearly identical to those produced by WT Jurkat T cells (Fig. 7 G). Therefore, the CPI motif is dispensable for co-stimulation via CD28 in Jurkat T cells.

The CPI motif of mouse RLTPR molecules is dispensable for co-stimulation via CD28 and the development of T reg cells

Much of the previous efforts aiming at unraveling the function of LRRC16 protein family focused on the CPI motif, as its ability to decrease the affinity of CP for actin

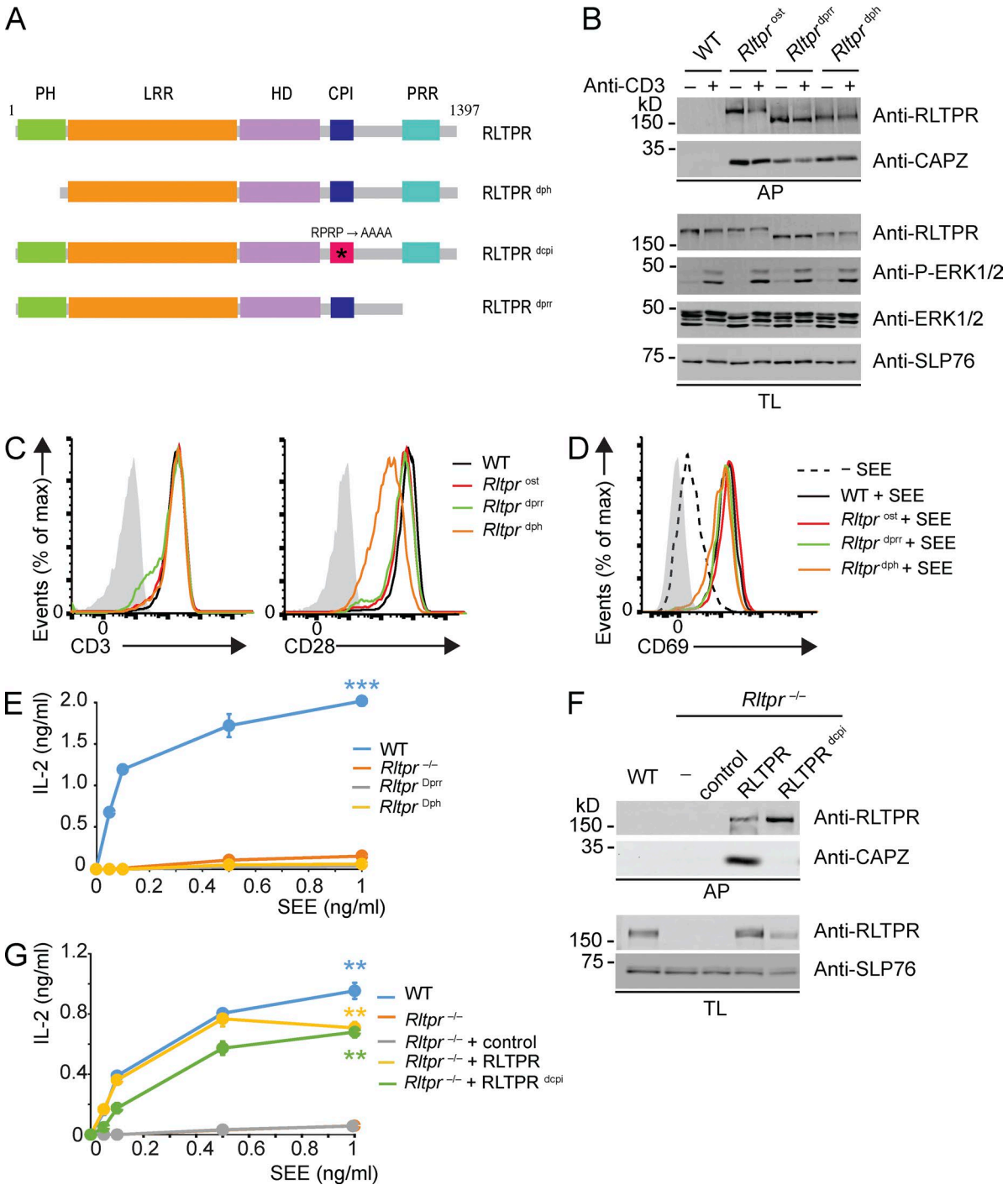

Figure 7. **Role of the PH domain, CPI motif, and PRR region of RLTPR during CD28 co-stimulation of Jurkat cells.** (A) Domain organization of RLTPR and structure of the engineered RLTPR mutations. RLTPR comprises an N-terminal noncanonical PH domain, a LRR domain, a putative HD, and an extended C terminus that contains a CPI motif and a proline-rich region (PRR). (B) WT, *Rltpr*^{ost}, *Rltpr*^{dprr}, and *Rltpr*^{dph} Jurkat cells were left untreated (–) or stimulated (+) with anti-CD3 for 2 min at 37°C. Immunoblot analysis of equal amounts of lysates from the specified cells were subjected to affinity purification (AP) on Strep-Tactin-Sepharose beads, followed by elution of proteins with D-biotin, and probed with anti-RLTPR and anti-CAPZ. Also shown is immunoblot analysis of equal amounts of total lysates (TL) of the specified cells probed with anti-RLTPR, anti-phospho-ERK1/2 (anti–P-ERK1/2), anti-ERK1/2, and anti-SLP76 (as a loading control). (C) Expression of CD3ε and CD28 on WT and *Rltpr*^{ost}, *Rltpr*^{dprr}, and *Rltpr*^{dph} Jurkat cells. Gray shaded curves, isotype-matched control antibody (negative control). (D) RLTPR-sufficient (WT) and *Rltpr*^{ost}, *Rltpr*^{dprr}, and *Rltpr*^{dph} Jurkat cells were stimulated with Raji cells in absence (– SEE) or presence (+ SEE) of SEE. For each condition, CD69 up-regulation was measured by FACS 24 h after stimulation. (E) IL-2 production by WT and *Rltpr*^{ost}, *Rltpr*^{dprr}, and *Rltpr*^{dph} Jurkat cells stimulated for 24 h with Raji cells and SEE at different concentrations. (F) Im-

filament was considered as a cardinal attribute of such protein family. Therefore, we sought to determine whether, as documented in human Jurkat T cells (Fig. 7, F and G), the CPI motif of RLTPR was also dispensable in mouse primary T cells for co-stimulation via CD28 and the development of T reg and effector memory $CD4^+$ T cells. We generated mice containing the very same mutation as that affecting the CPI motif in *Rltpr*^{dcpi} Jurkat cells (Fig. S4 A). Mice homozygous for this mutation, *Rltpr*^{dcpi} (also known ad B6-*Rltpr*^{tm4Mal}), were born at the expected Mendelian frequencies. Akin to *Rltpr*$^{bas/bas}$ mice, their T cells contained approximately twofold less RLTPR protein than WT *Rltpr*$^{+/+}$ mice (Fig. S4 B), suggesting that the constitutive association of RLTPR to CP increases its stability. *Rltpr*$^{dcpi/dcpi}$ mice showed a normal sequence of T cell development and their periphery was populated by normal numbers of $CD4^+$ and $CD8^+$ T cells with a normal phenotype (Fig. 8, A and B; and Fig. S4, C and E). In contrast to *Rltpr*$^{bas/bas}$ and *Rltpr*$^{-/-}$ mice, the spleen of *Rltpr*$^{dcpi/dcpi}$ mice contained numbers of T reg cells and of $CD44^{hi}$ $CD62L^{lo}$ effector memory T cells identical to those of WT mice (Fig. 8, C and D; and Fig. S4, F and G). T cells from *Rltpr*$^{dcpi/dcpi}$ mice were stimulated with a suboptimal dose of anti-CD3 in the presence or absence of anti-CD28. Analysis of the resulting T cell proliferation and IL-2 production showed that the RLTPR^{DCPI} molecules did not prevent CD28 from acting in synergy with the TCR–CD3 complex (Fig. 8, E and F). Therefore, as observed in human Jurkat T cells, the CPI motif of mouse RLTPR molecules is dispensable for co-stimulation via CD28 and the development of T reg and effector memory $CD4^+$ T cells.

The CPI motif of RLTPR is dispensable for RLTPR-dependent CD28 internalization

CD28 is rapidly internalized after ligation, and we previously showed that T cells expressing RLTPR^{BAS} molecules had more antibody-induced internalization of CD28 than T cells expressing WT RLTPR molecules (Liang et al., 2013). Likewise, T cells deprived of RLTPR had more antibody-induced internalization of CD28 than WT T cells (Fig. 8 G). In contrast, T cells expressing RLTPR^{DCPI} molecules have the same rate of CD28 internalization as WT T cells. Therefore, breaking the linkage between RLTPR and CPs had no detectable effect on the internalization of CD28. Conversely, mutating the LRR domain or eliminating RLTPR likely diminished the drag through the cytosol and enhanced the internalization of CD28.

Comparative functional analysis of RTLPR deficiency in mouse and human

The patients reported in the companion paper by Wang et al. (2016) harbor either a homozygous nonsense *Rltpr* allele leading to no detectable RLTPR expression, or homozygous L372R or L525Q replacements in the RLTP LRR domain leading to low levels of protein expression as observed in *Rltpr*$^{bas/bas}$ mice. All those patients showed impaired Th1 and Th17 differentiation whereas Th2 differentiation was normal. To determine whether a similar phenotype occurred in mice, naive $CD4^+$ T cells from WT, *Rltpr*$^{-/-}$, and *Rltpr*$^{dcpi/dcpi}$ mice were analyzed in vitro for their capacity to differentiate into Th1, Th2, and Th17 cells. Determination of the absolute numbers of IFN-γ^+, IL-4^+, and IL-17^+ $CD4^+$ T cells produced under Th1-, Th2-, and Th17-polarizing conditions, respectively, showed that *Rltpr*$^{-/-}$ $CD4^+$ T cells gave rise to reduced number of Th1 and Th17 cells, whereas Th2 differentiation appeared to be unaffected (Fig. 9 A). *Rltpr*$^{dcpi/dcpi}$ $CD4^+$ T cells behaved like WT $CD4^+$ T cells in terms of Th differentiation, a result consistent with the normal CD28 signaling observed in those mice. Therefore, in both human and mouse, the lack of functional RLTPR molecules resulted in a failure of $CD4^+$ T cell to differentiate toward Th1 and Th17 fates, while leaving Th2 differentiation intact.

Considering that patients deprived of functional RLTPR molecules showed a paucity of memory B cells and poor antigen-specific antibody responses (Wang et al., 2016), *Rltpr*$^{bas/bas}$ mice were immunized with the T cell–dependent antigen TNP-KLH. The concentrations of anti-hapten antibodies determined after secondary immune responses were dramatically reduced as compared with WT mice (Fig. 9 B). Because RLTPR is also expressed in mouse B cells (Fig. 1), *Rltpr*$^{bas/bas}$ mice were also immunized with TNP-LPS, a T cell–independent antigen to measure intrinsic responsiveness of B cells to antigen. *Rltpr*$^{bas/bas}$ and WT mice showed similar responses to TNP-LPS (Fig. 9 C). Consistent with this last observation, cross-linking of the BCR of *Rltpr*$^{bas/bas}$ B cells with graded dose of $F(ab)'_2$ anti–mouse IgM antibody induced their proliferation to the same extent as WT B cells (Fig. 9 D). Likewise, compared with WT B cells, proliferation of *Rltpr*$^{bas/bas}$ B cells was normal in response to LPS or to CD40 stimulation in the presence or absence of BCR cross-linkage (Fig. 9 D). *Rltpr*$^{dcpi/dcpi}$ B cells also behaved as WT B cells. Therefore, despite the fact that RLTPR is expressed in mouse B cells, the poor T cell–dependent B cell responses observed in *Rltpr*$^{bas/bas}$ mice are likely a result of the essential role RLTPR plays in mouse T cells.

munoblot analysis of RLTPR-deficient (*Rltpr*$^{-/-}$) Jurkat cells before (–) and after retroinfection with an empty vector (control) or vectors containing WT *Rltpr* (RLTPR) or *Rltpr*^{dcpi} (RLTPR^{dcpi}) cDNA. Equal amounts of lysates were subjected to affinity purification (AP) on Strep-Tactin-Sepharose beads, followed by elution of proteins with D-biotin, and probed with anti-RLTPR and anti-CAPZ. Also shown is immunoblot analysis of equal amounts of total lysates (TL) of the same cells probed with anti-RLTPR and anti-SLP76 (loading control). (G) IL-2 production by the cells specified in E 24 h after stimulation with Raji cells and SEE at indicated concentrations. Data are representative of three independent experiments (E and G, mean and SEM are shown; **, $P \leq 0.01$; ***, $P \leq 0.001$).

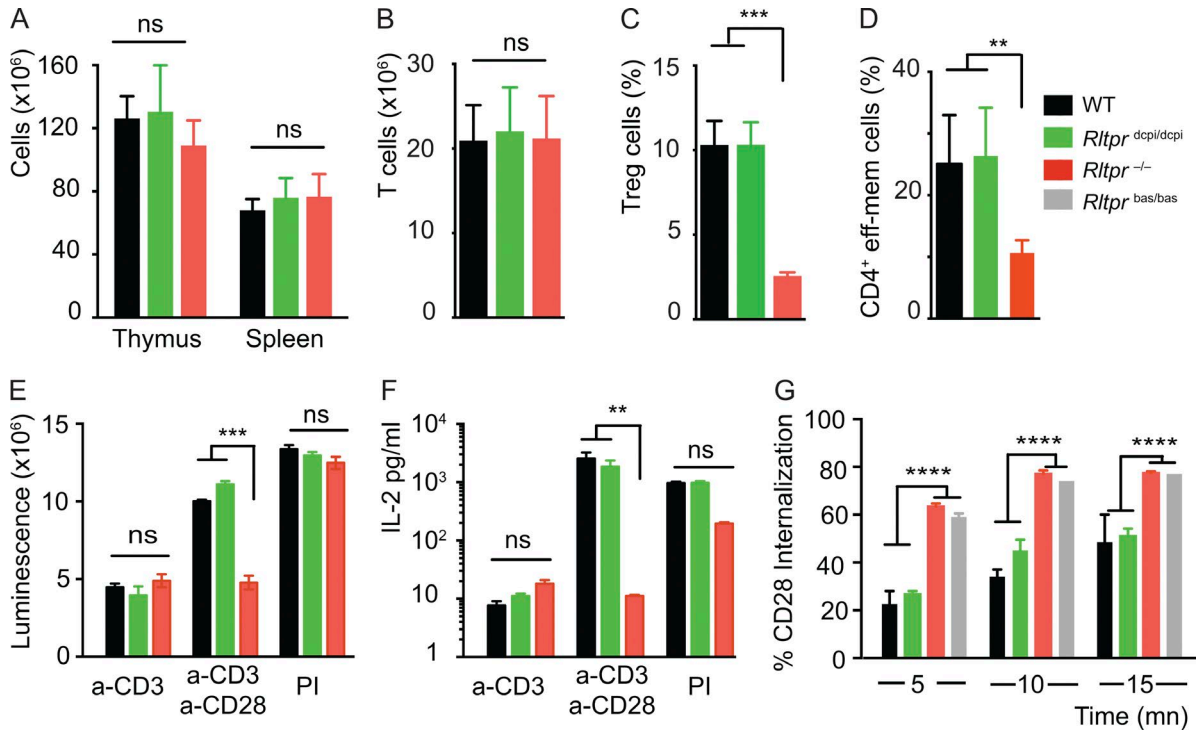

Figure 8. **The mouse RLTPR CPI motif is dispensable for co-stimulation via CD28 and the development of T reg cells.** (A) Cellularity of thymus and spleen of WT, *Rltpr*$^{dcpi/dcpi}$, and *Rltpr*$^{-/-}$ mice (key: top right corner). (B) Quantification of T cells in the spleen of WT, *Rltpr*$^{dcpi/dcpi}$, and *Rltpr*$^{-/-}$ mice. (C) Percent T reg cells in WT, *Rltpr*$^{dcpi/dcpi}$, and *Rltpr*$^{-/-}$ spleen. (D) Percent CD4^{+} effector memory (CD44^{+}CD62L^{lo}) cells in WT, *Rltpr*$^{dcpi/dcpi}$, and *Rltpr*$^{-/-}$ spleen. (E) ATP content of negatively purified CD4^{+} T cells from lymph nodes of WT, *Rltpr*$^{dcpi/dcpi}$, and *Rltpr*$^{-/-}$ mice, activated for 48 h in vitro with plate-bound anti-CD3 in the presence or absence of soluble anti-CD28 or with PMA and ionomycin (PI), assessed as luminescence. (F) IL-2 in supernatants of purified WT, *Rltpr*$^{dcpi/dcpi}$, and *Rltpr*$^{-/-}$ CD4^{+} T cells activated for 48 h, as in E. (G) Internalization of CD28 by WT, *Rltpr*$^{dcpi/dcpi}$, *Rltpr*$^{bas/bas}$, and *Rltpr*$^{-/-}$ peripheral T cells after cross-linkage for 5, 10, or 15 min. Results are presented as percent change in surface CD28 expression relative to that at time 0. Data representative of two experiments with three mice per group (mean and SEM). **, P ≤ 0.01; ***, P ≤ 0.005; ****, P ≤ 0.001; ns, nonsignificant.

DISCUSSION

We demonstrated that RLTPR acts as a scaffold, bridging CD28 to CARMA1, and as such is essential for CD28 co-stimulation in mouse T cells and in the human leukemic T cell line Jurkat, a finding consistent with in vivo and ex vivo analysis of T cells from patients with inherited RLTPR deficiency (Wang et al., 2016). Mouse RLTPR is also expressed in B cells, long-lived plasma cells, NK cells, and pDCs, and analysis of human circulating leukocytes revealed a rather similar pattern of RLTPR expression (Wang et al., 2016). In both species, the pattern of expression of CD28 largely correlated with that of RLTPR, suggesting that the CD28-RLTPR functional linkage first documented in T cells (Liang et al., 2013) extends to other types of leukocytes. Loss of CD28 activation significantly diminishes humoral responses (Shahinian et al., 1993; Dodson et al., 2009), a finding originally attributed to defective T cell help. However, a recent study showed that CD28 provides signals that enhance in a cell-autonomous manner the survival of long-lived plasma cells in the bone marrow (Rozanski et al., 2015), suggesting the possibility that such prosurvival signals are conveyed via a CD28–RLTPR signaling axis. As illustrated by both mouse and human B cells, RLTPR has a broader expression than that of CD28, pointing toward plausible CD28-independent function. Mice deprived of functional RLTPR molecules had normal numbers of B cells, and cross-linking of the BCR of such B cells induced their proliferation to the same extent as WT B cells. As a result, they responded normally to a T cell–independent antigen. Therefore, the reduced T cell–dependent B cell responses observed in the mouse in the absence of functional RLTPR molecules are likely caused by the essential role played by RLTPR in T cells. This differs from humans in which BCR-mediated B cell activation was affected in patients deprived of functional RLTPR molecules (Wang et al., 2016). Considering that mouse B cells coexpress LRRC16A in addition to RLTPR, it remains possible that the mouse BCR differs from its human counterpart in that it uses RLTPR and LRRC16A in a redundant manner. In mouse pDC, CD28 acts as a negative regulator of type I IFN production after TLR stimulation or viral infection (Macal et al., 2016). In contrast, CD28 promotes activation and cytotoxicity of NK cells (Galea-Lauri et al., 1999). Although, mice deprived of RLTPR had normal numbers of pDC and NK cells (un-

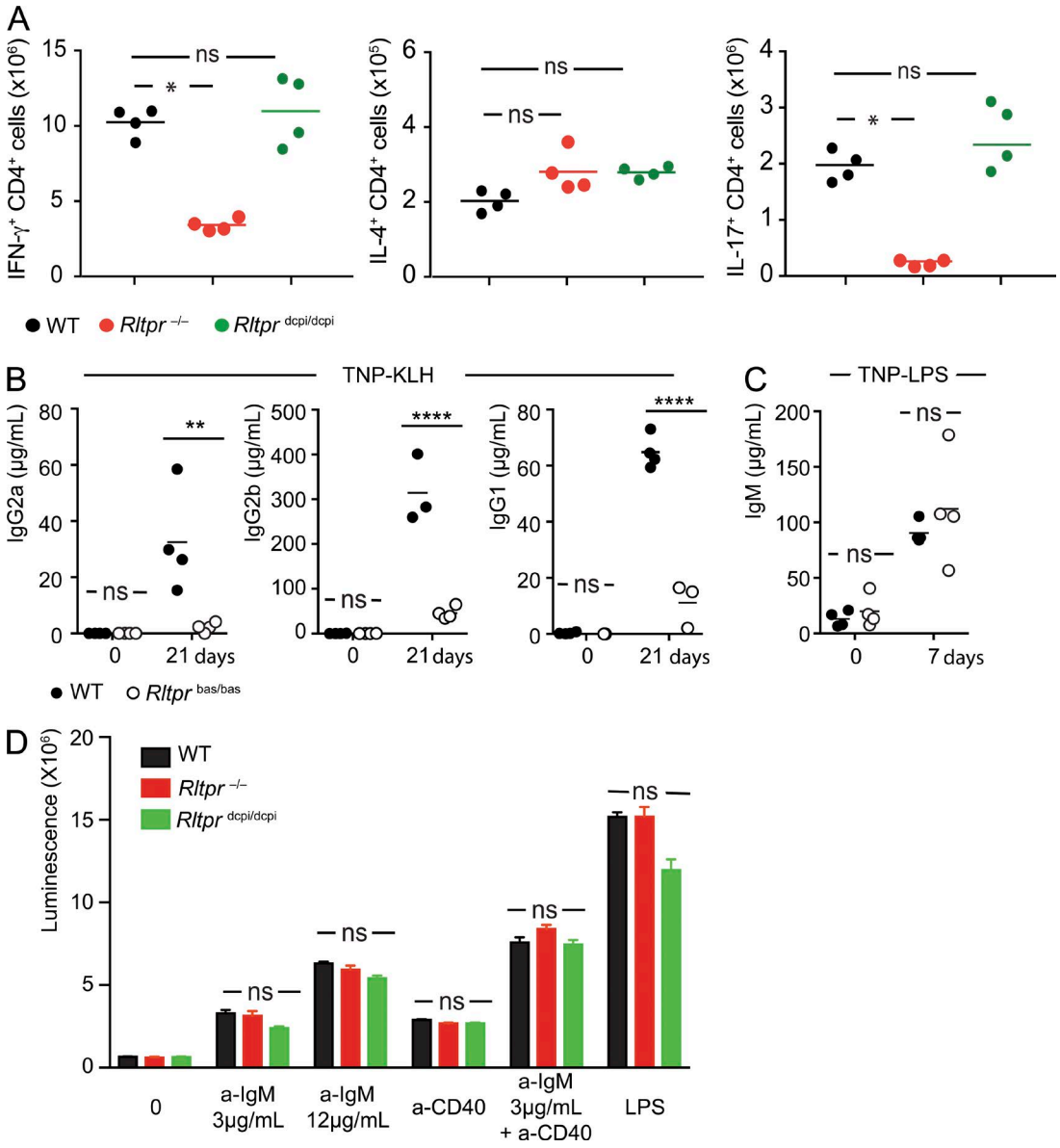

Figure 9. **Th differentiation and B cell responses in mice deprived of functional RLTPR molecules.** (A) Sorted naive CD4$^+$ T cells (2×10^5) from mice of the specified genotype were stimulated for 5 d with anti-CD3 and -CD28 under Th1, Th2, or Th17 differentiating conditions. After 5 d of culture, the absolute number of IFN-γ$^+$ (Th1 condition), IL-4$^+$ (Th2 condition), and IL-17$^+$ (Th17 condition) CD4$^+$ T cells was determined. Each dot corresponds to a mouse and the mean (horizontal bar) is indicated. (B) WT and *Rltpr*$^{bas/bas}$ mice were immunized intraperitoneally at day 0 and 14 with the T cell–dependent antigen TNP-KLH. The concentration of TNP-specific immunoglobulins of the indicated isotypes (IgG2a, IgG2b, and IgG1) were assessed in individual mice before and 21 d after immunization. (C) WT and *Rltpr*$^{bas/bas}$ mice were immunized with the T cell–independent antigen TNP-LPS, and the concentration of TNP-specific IgM was assessed in individual mice before and 7 d after immunization. (D) Splenic B cells from mice of the specified genotype were stimulated with F(ab)'$_2$ goat anti–mouse IgM antibody in the presence or absence of anti-CD40 antibody, or LPS. After 4 d of culture, B cell proliferation was evaluated. Mean and SEM are shown. Data are representative of two independent experiments. In A–C, each dot corresponds to a mouse and the mean (horizontal bar) is indicated. **, $P \leq 0.01$; ****, $P \leq 0.001$; ns, nonsignificant. In D, two animals were used per genotype.

published data), it remains to be determined whether CD28 uses RLTPR to signal in pDC and NK cells. If applicable to humans, such information should help determine whether the pathological conditions afflicting RLTPR-deficient patients result from malfunction in leukocytes other than T and B cells.

Using Jurkat leukemic T cells and mouse primary T cells, which constitute the cellular environment in which RLTPR operates normally, we analyzed the functional role of the various structural domains identified to date in the RLTPR molecule. Deletion of the noncanonical PH domain

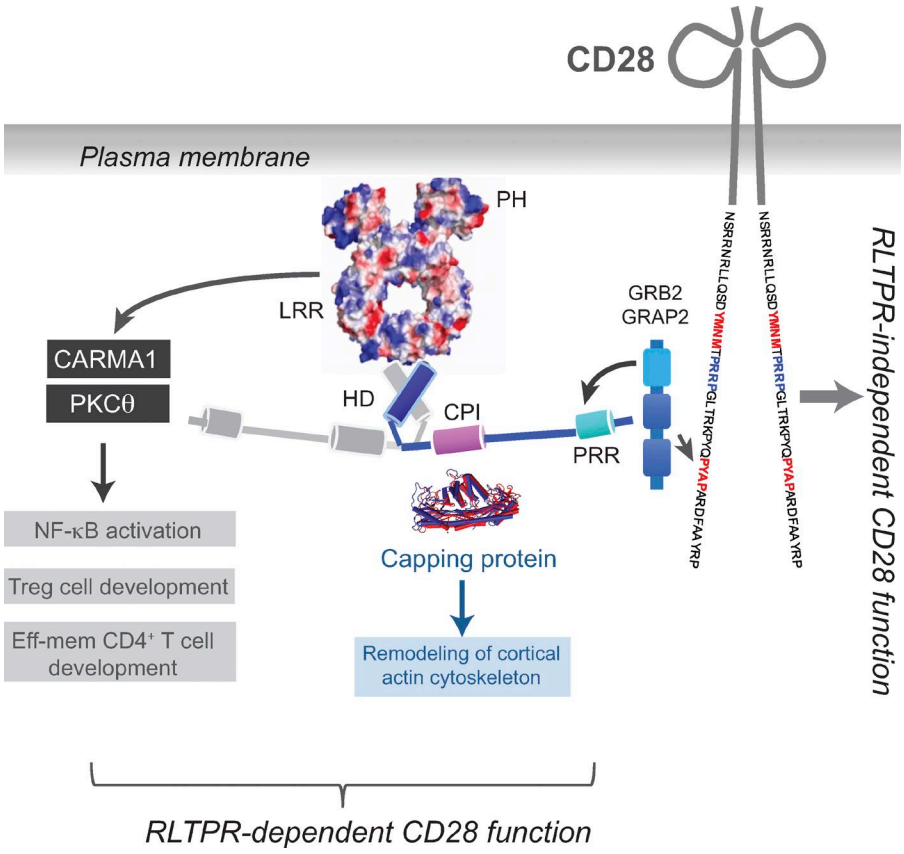

Figure 10. **A model illustrating the mode of action of RLTPR in T cells.** RLTPR is required for coupling CD28 to PKC-θ and CARMA-1, two proximal effectors of the CD28 signaling pathway. RLTPR exists as constitutive dimer and contains a putative HD. The CPI motif of RLTPR molecules is constitutively associated with a CP, conferring actin-uncapping properties to RLTPR molecules. As a result, RLTPR molecules are thought to remodel the cortical actin cytoskeleton upon T cell activation. Our data demonstrated, however, that the RLTPR CPI motif is dispensable for co-stimulation via CD28 and the development of T reg and effector memory CD4+ T cells. In contrast, the LRR domain, the noncanonical PH domain, and the PRR of RLTPR are each mandatory for co-stimulation via CD28. By disrupting the structure of the LRR domain, the L432 mutation found in *Rltpr*^{bas} mice prevents the association of RLTPR with CARMA1, thereby abrogating CD28-mediated co-stimulatory signals. Whether the PRR region of RLTPR is coupled to the PYAP motif found in the CD28 cytoplasmic tail via the GRB2 or GRAP2 adaptors remains to be demonstrated. CD28 likely exerts both RLTPR-dependent and -independent functions.

found in mouse LRRC16A reduced its localization at the plasma membrane (Zwolak et al., 2013). Sequence alignment suggests that RLTPR contains a similar noncanonical PH domain. However, the residues present in the LRRC16A noncanonical PH domain and necessary for membrane binding are not conserved in the corresponding PH domain of human and mouse RLTPR, preventing its use for plasma membrane localization (Lanier et al., 2016). Instead, a 27-aa-long plasma membrane–binding motif located in close proximity to the RLTPR CPI motif and found necessary for endocytic and migratory functions of fibrosarcoma cells (Lanier et al., 2015). Regardless of the exact function of the 158 aa found at the N terminus of RLTPR, our analysis of *Rltpr*^{dph} Jurkat T cells stresses their functional importance in CD28 co-stimulation.

LRR domains are frequently involved in the formation of protein–protein interactions. Here, we formally established that the RLTPR LRR domain has an essential functional role in CD28 co-stimulation. The mutation found in the LRR of RLTPR^{BAS} molecules did not prevent the formation of CD28-RLTPR microclusters, but blocked their colocalization with CARMA1 at the immune synapse (Liang et al., 2013). When considered together with our AP-MS analysis showing that RLTPR associates with both CD28 and CARMA1, the aforementioned results suggest that the LRR domain of RLTPR directly or indirectly associates with CARMA1 (Fig. 10). The LRR domain of LRRC16A is composed of repeating units with a β-strand-turn-α-helix structure and has a horseshoe shape with a solvent accessible concave interior surface made of parallel β-strands and a convex exterior surface made of array of α-helices (Zwolak et al., 2013). In the event that the LRR domain of RLTPR shows the same structure as that of LRRC16A, the L432P mutation identified in the mouse *Rltpr*^{bas} allele and two of the mutations identified in human RLTPR (L372R and L525Q) are located within the LRR β-strands. The receptor for the FSH glycoprotein hormone uses the β-strands of the concave surface of its LRR domain to recognize FSH (Fan and Hendrickson, 2005). Provided that RLTPR uses a similar strategy to bind to CARMA1, the nonconservative substitutions L432P, L372R, and L525Q likely disrupt the organization of the concave surface and prevent the association with CARMA1. Alternatively, those mutations may indirectly impact on the convex and fully exposed LRR surface. Upon heterologous expression in a fibrosarcoma cell line, the LRR domain of RLTPR was found to be necessary for its colocalization with the vimentin intermediate filament network (Lanier et al., 2016). However, our AP-MS analysis, conducted in T cells, failed to recover vimentin-specific peptides.

The CD28 cytoplasmic segment contains a YMNM motif and two proline-rich motifs (PRRP and PYAP), the relative contribution of which to CD28 co-stimulatory function remains debated (Okkenhaug et al., 2001; Raab et

al., 2001; Kong et al., 2011; Pagán et al., 2012). GRB2 and GRAP2 are capable of binding to the YMNM and PYAP motifs found in the CD28 cytoplasmic segment (Higo et al., 2014), and both are found in the RLTPR interactome after T cell activation. Analysis of RLTPR-OST molecules present in lysates of pervanadate-stimulated thymocytes showed no detectable tyrosine phosphorylation (not depicted and Tian et al., 2015). Therefore, provided that GRB2 and GRAP2 bind directly to RLTPR, this should occur via their SH3 domains and involve the C-terminal PRR region of RLTPR. The C-terminal PRR region is essential for co-stimulation via CD28 in Jurkat T cells (this study), and ablation of the CD28 PYAP motif mimics a RLTPR deficiency in that it prevents both T reg cell development (Vang et al., 2010) and survival of long-lived plasma cells in mouse bone marrow (Rozanski et al., 2015). Therefore, GRB2 and/or GRAP2 likely couple the RLTPR PRR region to the CD28 PYAP motif (Fig. 10).

Although most previous studies aiming at unraveling the function of LRRC16 family proteins focused on the CPI motif, our data using human Jurkat T cells and mouse primary T cells demonstrated that the RLTPR CPI motif was dispensable for co-stimulation via CD28 and the development of T reg and memory-effector $CD4^+$ T cells. It has been suggested that CD28 plays an important role in regulating the actin cytoskeleton (Liang et al., 2013; Tan et al., 2014; Lanier et al., 2015). For instance, when a T cell encounters an APC bearing its cognate peptide–MHC ligand, the LCK protein-tyrosine kinase initiates a tyrosine phosphorylation cascade that leads to the phosphorylation and activation of phospholipase PLC-γ1 and to the assembly of a CD28 signalosome. Ensuing CD28 signals are thought to remodel the cortical actin at the site of active TCR signaling, enabling LAT-bound PLC-γ1 to access phosphatidylinositol-4,5 bisphosphate at the plasma membrane and convert it into inositol trisphosphate and diacylglycerol. Although our analysis of human and mouse $RLTPR^{DCPI}$ molecules suggests that an actin component is not required for RLTPR-mediated CD28 co-stimulation, the recent discovery that CapZIP, another CPI motif-containing protein, is required for CD28 co-stimulation-dependent IL-2 production (Tian et al., 2015) suggests that CapZIP can compensate for $RLTPR^{DCPI}$ molecules. Other, yet to be analyzed, functions of RLTPR might depend on its actin-uncapping activity. For instance, both the *Rltpr*^{bas} mutation and the ablation of the Wiscott-Aldrich Syndrome Protein (WASP) do not affect the overall accumulation of F-actin at the immunological synapse (Liang et al., 2013; Lanier et al., 2015). However, the lack of WASP affected F-actin foci that constitute a minute fraction of total synaptic F-actin (Lanier et al., 2015). DOCK8, a member of the DOCK180 family of guanine nucleotide exchange factors, is part of the RLTPR interactome. Remarkably, it is only when they migrate through confined spaces that DOCK8-deficient T and NK cells develop cell shape deformation abnormalities that impair their viability (Zhang et al., 2014). Disentangling the actin-uncapping function of RLTPR may thus require testing of T cells subjected to a mechanically constrained environment. Therefore, the structure–function analysis of RLTPR allowed us to build a more complete model of how RLTPR contributes to CD28 co-stimulation in both mouse and human T cells, emphasizing its role as a scaffolding protein capable of interacting with CD28 and CARMA1 independent of its actin-uncapping function (Fig. 10).

In conclusion, although *Rltpr*$^{bas/bas}$ and *Rltpr*$^{-/-}$ mice contain normal numbers of conventional T cells and diminished numbers of T reg cells, they developed no blatant autoimmune manifestations, which is consistent with RLTPR-deficient patients (Wang et al., 2016). This paradox—also raised in the case of CARMA1-deficient mice (Vang et al., 2010)—can be accounted for by the coincident defect in CD28 co-stimulation that plagues the conventional T cells that develop in normal numbers in *Rltpr*$^{bas/bas}$ and *Rltpr*$^{-/-}$ mice and, in turn, leads to a paucity of effector memory T cells. This view is consistent with the primary function of T reg cells, which is to oppose CD28 signaling by down-regulating CD80 and CD86 on APC (Soskic et al., 2014). Recent developments in MS applied to activated mouse $CD8^+$ T cells have revealed that the number of CD28 molecules per activated mouse $CD8^+$ T cell (1.2×10^4) is higher than that of RLTPR (2.6×10^3; Hukelmann et al., 2016). Assuming that the whole pool of RLTPR is available for engaging in interaction with CD28, at most 20% of the CD28 molecules present at the T cell surface will be associated with RLTPR. Therefore, although RLTPR-bound CD28 molecules constitute a few needles in the CD28 haystack, it is those molecules that are functionally relevant in term of co-stimulation. Owing to their minute numbers, they likely exert their function in a rather local manner at the immune synapse, and their functional importance may have gone unnoticed without combining functional genomics and proteomics. Therefore, our study illustrates how integrative biology of T cell activation (Malissen et al., 2014) helps in delineating the dynamic relationships between signaling protagonists in the T cell interior to provide a more complete model of CD28 co-stimulation in human and mouse, in which RLTPR has a critical role.

MATERIALS AND METHODS

Mice

Rltpr^{bas} (B6-*Rltpr*^{bas}) and *Cd28*$^{-/-}$ (B6.129S2-*Cd28*^{tm1Mak}) mice have been previously described (Shahinian et al., 1993; Liang et al., 2013). Generation of the *Rltpr*^{ost} (B6-*Rltpr*^{tm1Mal}), *Rltpr*$^{-}$ (B6-*Rltpr*^{tm2Mal}), and *Rltpr*^{dcpi} (B6-*Rltpr*^{tm4Mal}) gene-targeted mice is described in Figs. S1, S3, and S4. Mice were maintained in specific pathogen–free conditions.

Animal experimental guidelines

Mice were handled in accordance with national and European laws for laboratory animal welfare and experimentation (EEC Council Directive 2010/63/EU, September 2010), and all protocols were approved by the Marseille Ethical Committee for Animal Experimentation (Comité National de Réflexion Ethique sur l'Expérimentation Animale no. 14).

Construction of an OST-(Stop)$_2$-IRES2-mTFP1-LoxP-frt-neo^r-frt cassette

A cassette containing a One-STrEP-tag (OST) sequence (Junttila et al., 2005), two STOP codons, an IRES2 sequence (from pIRES2-EGFP; Takara Bio Inc.), a Kozak sequence and a sequence coding for mTFP1, a monomeric, bright, and photostable version of *Clavularia* cyan fluorescent protein (Ai et al., 2006), was abutted to a frt-flanked cassette that contains a neomycin-kanamycin resistance (*neo*^{r}) gene that can be expressed under the control of a prokaryotic (gb2) or eukaryotic (*Pgk1*) promoter.

Targeting vector for *Rltpr^{ost}* allele

A 12.5-kb genomic fragment containing the 3′ end of the *Rltpr* gene was isolated from a BAC clone (clone no RP23-70F13; Life Sciences) of C57BL/6J origin. Using ET recombination (Zhang et al., 2000), an OST-(Stop)$_2$-IRES2-mTFP1-loxP-frt-neo^r-frt cassette (see previous section) was appended in frame at the 3′ end of the coding sequence of the *Rltpr* gene. An frt3-puro^r-frt3-LoxP cassette was also introduced in the intron located between exons 23 and 24.

Targeting vector for *Rltpr$^-$* allele

The targeting construct used for the disruption of the *Rltpr* gene consists of a self-excising ACN cassette (Bunting et al., 1999) in place of exons 1–3 of the *Rltpr* gene and of two homology arms of 2.5 kb that bracket the sequence to be deleted. The targeting construct was abutted to a cassette coding for the diphtheria toxin fragment A (Soriano, 1997).

Targeting vector for *Rltpr^{dcpi}* allele

Such targeting construct was intended to change into alanine 4-aa residues (RPRP) found in the middle of the CPI motif coded by exon 30 of the *Rltpr* gene. It comprised a 1,384-bp 5′ homology arm and a 1,219-bp 3′ homology arm bracketing the mutated target sequence in exon 30. A self-excising ACN cassette was introduced in the intron flanking the 3′ end of exon 30 and the final targeting construct was abutted to a cassette coding for the diphtheria toxin fragment A.

Isolation of recombinant ES cell clones

JM8.F6 C57BL/6N ES cells (Pettitt et al., 2009) were electroporated with the targeting vectors. After selection in G418 alone (*Rltpr$^-$* and *Rltpr^{dcpi}*) or in G418 and puromycin (*Rltpr^{ost}*), ES cell clones were screened for proper homologous recombination by Southern blot analysis. For the *Rltpr^{ost}* allele, when tested on BamHI-digested genomic DNA, the 5′ single-copy probe used to identify proper recombination events hybridized to a 7.7-kb WT fragment and to a 9.7-kb recombinant fragment. When tested on *Asp718*-digested genomic DNA, the 3′ single-copy probe used to identify proper recombination events hybridized to an 8.3-kb WT fragment and to a 5.8-kb recombinant fragment. For the *Rltpr$^-$* allele, when tested on *Xba1*-digested genomic DNA, the 5′ single-copy probe used to identify proper recombination events hybridized to a 9.0-kb WT fragment and to a 5.1-kb recombinant fragment. When tested on *Xba1*-digested genomic DNA, the 3′ single-copy probe used to identify proper recombination events hybridized to a 9.0-kb WT fragment and to a 3.3-kb recombinant fragment. For *Rltpr^{dcpi}*, when tested on *Dra1*-digested genomic DNA, the 5′ and 3′ single-copy probes used to identify proper recombination events hybridized to a 4.9-kb WT fragment and to an 8.6-kb recombinant fragment. A *neo^r*-specific probe was used to ensure that adventitious nonhomologous recombination events have not occurred in the selected *Rltpr^{ost}*, *Rltpr$^-$*, and *Rltpr^{dcpi}* ES clones.

Production of knock-in mice

Mutant ES cells were injected into FVB blastocysts. In the case of the *Rltpr^{ost}* allele, excision of the frt-neo^r-frt and frt3-puro^r-frt3 cassettes was achieved through genetic cross with transgenic mice expressing the FLP recombinase under the control of the actin promoter (Rodríguez et al., 2000). For *Rltpr^{ost}*, screening for the proper deletion of the frt-neo^r-frt cassette and for the presence of the OST-(Stop)$_2$-IRES2-mTFP1-LoxP-frt sequence was performed by PCR using the following pair of primers: sense 5′-GCCTTGGATCCA AGCCTCTTCCTC-3′ and antisense 5′-TGCCCGTGT TGGTCACCAGT-3′ (WT allele) or 5′-GCCTGCAAA GGGTCGCTACA-3′ (*Rltpr^{ost}* allele). They amplified a 351-bp band in the case of the WT *Rltpr* allele and a 503-bp band in the case of the *Rltpr^{ost}* allele. Note that the *Rltpr^{ost}* allele is a multitask allele permitting (1) affinity purification of the RLTPR protein, (2) conditional deletion of the *Rltpr* gene, and (3) visualization of cells expressing the *Rltpr* gene. Affinity purification was the only functionality used in this study. We failed establishing mice homozygous for the *Rltpr^{ost}* allele. Analysis of the 3′ untranslated of the *Rltpr* gene revealed that the reverse strand codes for the 3′ end of the *Acd* gene. This gene encodes a protein that is involved in telomere function and its constitutive ablation resulted in lethality (Kibe et al., 2010). Accordingly, it is likely that the introduction of the OST-(Stop)$_2$-IRES2-mTFP1-LoxP-frt cassette in the 3′ end of the *Rltpr* gene adventiously affected the expression of the *Acd* gene and prevented establishment of mice homozygous for the *Rltpr^{ost}* allele. For *Rltpr$^-$*, screening for the proper deletion of the ACN cassette and for the presence of the expected deletion of exons 1–3 was performed by PCR. The pair of primers used were: sense 5′-ACTACGGGG CAGGGTGGAAGTA-3′ and antisense 5′-GGTGACTTT GGCTCCTCTATTAGGGC-3′ amplified a 613-bp band in the WT allele, whereas the pairs of primers: sense 5′-ACT ACGGGGCAGGGTGGAAGTA-3′ and antisense 5′-TGA GCTAGACCTGCCCAGACTTCCC-3′ amplified a 475-bp band in the *Rltpr$^-$* allele. For *Rltpr^{dcpi}*, screening for the proper deletion of the ACN cassette and for the presence of the expected mutation that is tagged by the LoxP site left in the intron flanking the 3′ end of exon 30 was performed by PCR using the following pair of primers: sense 5′-GTG

CTGCTGAGGAAGCGGAA-3′ and antisense 5′-GAG GGTGGCCAGAAAGATGA-3′. It amplified a 377-bp band in the case of the WT allele and a 462-bp band in the case of the *Rltpr*^{dcpi} allele.

Generation of an anti-RLTPR monoclonal antibody

BALB/c mice were immunized with a glutathione S-transferase (GST) fusion protein encompassing aa 1147–1397 of mouse RLTPR. A monoclonal antibody denoted as EM-53 (IgG1, κ) and recognizing GST-RLTPR$^{1147\text{-}1397}$ but not GST was selected. Immunoblot analysis of lysates from T cells isolated from WT mice showed that the antibody recognized a single protein species of ∼150-kD—the molecular weight expected for RLTPR—that was lacking in RLTPR-deficient T cells (Fig. S2 B). Mouse B cells coexpress RLTPR and LRRC16A, a protein coded by a paralog of the *Rltpr* gene family. Intracellular staining of B cells from RLTPR-sufficient and -deficient mice showed that the EM-53 mAb did not recognize LRRC16A (Fig. 1 C). Therefore, the EM-53 mAb specifically recognized mouse RLTPR molecules. Using RLTPR-sufficient and -deficient human Jurkat T cells, EM-53 was found to cross-react with human RLTPR (Fig. 5 C). EM-53 also reacted with RLTPR^{dprr} molecules (Fig. 7 A), suggesting that its epitope is located within the amino acid sequence corresponding to residues 1147–1272.

Flow cytometry

Stained cells were analyzed using a LSRII system and FAC SDiva 8.1 software (BD). Cell viability was evaluated using SYTOX Blue (Life Technologies) or Aqua Dead (Molecular Probes). The following antibodies were used: anti-CD3 (145-2C11), anti-CD4 (RMA-5), anti-CD5 (53–7.3), anti-CD8 (53–6.7), anti-CD11b (MI/70), anti-CD28 (37.51), anti-CD44 (IM7), anti-CD45R (RA3-6B2), anti-CD62L (MEL-14), anti-CD138 (281–2), anti-Ly-6G (1A8), and anti-TCRβ (H57-597), all purchased from BD; anti-CD24 (M1/69), anti-CD25 (PC61.5), anti-CD27 (LG3A10), anti-CD19 (6D5), anti-CD161 (PK136), anti-SiglecH (551), all obtained from BioLegend; and anti-CD317 (927), anti-Foxp3 (FJK-16s), and anti-TCRδ (GL-3), all purchased from eBioscience. A CellTiter-Glo Luminescent Cell Viability Assay (Promega) was used for assessing T cell proliferation. It is based on quantification of the ATP present in the medium and is directly proportional to the number of living cells in the well. After the specified time of culture, 100 µl of CellTiter-Glo reagent (Promega) was added directly to each well. The resulting luminescence, proportional to the ATP content of the culture, was measured using a Victor2 luminometer (Wallac; Perkin Elmer Life Science). IL-2 production was measured using Cytometric Bead Array (BD). Jurkat T cells were analyzed using anti-CD3 (UCHT1), anti-CD28 (L293), and anti-CD69 (L78) purchased from BD.

Thymocyte stimulation and lysis

Thymocytes (100×10^6) from *Rltpr*^{ost} and WT mice were left unstimulated or stimulated at 37°C with pervanadate for 30, 120, 300, and 600 s. Pervanadate stock solution was made by mixing 7.6 volumes of water with 1.9 volumes of hydrogen peroxide (10 mM final concentration), and with 0.5 volume of sodium orthovanadate (100 µM final concentration), and left for 15 min at 20°C before addition to thymocytes. Stimulation was stopped by the addition of lysis buffer (50 mM Tris, 1% Nonidet P-40, 2 mM EDTA) supplemented with protease and phosphatase inhibitors. After 10 min of incubation on ice, cell lysates were centrifuged at 20,000 *g* for 5 min at 4°C. Postnuclear lysates were used for affinity purification or immunoblot analysis.

Affinity purification of protein complexes

Equal amount of postnuclear lysates were incubated with prewashed Strep-Tactin Sepharose beads (IBA GmbH) for 1.5 h at 4°C on a rotary wheel. Beads were then washed five times with 1 ml of lysis buffer in the absence of detergent and of protease and phosphatase inhibitors. Proteins were eluted from the Strep-Tactin Sepharose beads with 2.5 mM D-biotin.

MS analysis

Protein extracts were loaded on NuPAGE 4–12% bis-Tris acrylamide gels (Life Technologies) to stack proteins in a single band that was stained with Imperial Blue (Thermo Fisher Scientific) and cut from the gel. Gels pieces were submitted to an in-gel trypsin digestion (Shevchenko et al., 1996) with slight modifications. In brief, gel pieces were washed and destained using 100 mM NH_4HCO_3. Destained gel pieces were shrunk with 100 mM ammonium bicarbonate in 50% acetonitrile and dried at room temperature. Protein spots were then rehydrated using 10 mM DTT in 25 mM ammonium bicarbonate, pH 8.0, for 45 min at 56°C. This solution was replaced by 55 mM iodoacetamide in 25 mM ammonium bicarbonate, pH 8.0, and the gel pieces were incubated for 30 min at room temperature in the dark. They were then washed twice in 25 mM ammonium bicarbonate and finally shrunk by incubation for 5 min with 25 mM ammonium bicarbonate in 50% acetonitrile. The resulting alkylated gel pieces were dried at room temperature. The dried gel pieces were reswollen by incubation in 25 mM ammonium bicarbonate, pH 8.0, supplemented with trypsin (12.5 ng/ml; Promega) for 1 h at 4°C and then incubated overnight at 37°C. Peptides were harvested by collecting the initial digestion solution and carrying out two extractions; first in 5% formic acid, and then in 5% formic acid 60% acetonitrile. Pooled extracts were dried down in a centrifugal vacuum system. Samples were reconstituted with 0.1% trifluoroacetic acid in 4% acetonitrile and analyzed by liquid chromatography (LC)-tandem MS (MS/MS) in an LTQ-Orbitrap-Velos (Thermo Electron) online with a nanoLC Ultimate 3000 chromatography system (Dionex). Peptides were separated on a Dionex Acclaim PepMap RSLC C18 column. First, peptides were concentrated and purified on a precolumn (C18 PepMap100; Dionex; 2 cm × 100 µm I.D, 100 Å pore size, 5 µm particle size) in solvent A (0.1% formic acid in 2% acetonitrile). Next, peptides were

separated on a reverse phase column (C18 PepMap100; Dionex; 15 cm × 75 µm I.D, 100 Å pore size, 2 µm particle size) at 300 nl/min flow rate. After column equilibration using 4% of solvent B (20% water, 80% acetonitrile, and 0.1% formic acid), peptides were eluted from the analytical column by a two steps linear gradient (4–20% acetonitrile/H_2O; 0.1% formic acid for 90 min, and 20–45–45% acetonitrile/H_2O; 0.1% formic acid for 30 min).

For peptide ionization in the nanospray source, spray voltage was set at 1.4 kV and the capillary temperature at 275°C. The Orbitrap Velos was set up in data-dependent mode to switch consistently between MS and MS/MS. MS spectra were acquired with the Orbitrap in the range of m/z 400–1700 at a FWHM resolution of 30,000 measured at 400 m/z. For internal mass calibration, the 445.120025 ions were used as lock mass. The 10 abundant precursor ions were selected, and collision-induced dissociation fragmentation was performed in the ion trap on the 10 most intense precursor ions measured to have maximum sensitivity and yield a maximum amount of MS/MS data. The signal threshold for an MS/MS event was set to 500 counts. Charge state screening was enabled to exclude precursors with 0 and 1 charge states. Dynamic exclusion was enabled with a repeat count of 1, exclusion list size 500 and exclusion duration of 30 s.

Protein identification and quantification

Relative intensity-based label-free quantification (LFQ) was processed using the MaxLFQ algorithm (Cox et al., 2014) from the freely available MaxQuant computational proteomics platform, version 1.5.2.8 (Cox and Mann, 2008). The acquired raw LC Orbitrap MS data were first processed using the integrated Andromeda search engine (Cox et al., 2011). Spectra were searched against a SwissProt mouse database (version 2014.07). This database was supplemented with a set of 245 frequently observed contaminants. The following search parameters were used: (1) trypsin allowing cleavage before proline; (2) two missed cleavages were allowed; (3) monoisotopic precursor tolerance of 20 ppm in the first search used for recalibration, followed by 4.5 ppm for the main search and 0.5 D for fragment ions from MS/MS; (4) cysteine carbamidomethylation (+57.02146) as a fixed modification and methionine oxidation (+15.99491) and N-terminal acetylation (+42.0106) as variable modifications; (5) a maximum of five modifications per peptide allowed; and (6) minimum peptide length was 7 aa and a maximum mass of 4,600 D. The match between runs option was enabled to transfer identifications across different LC-MS/MS replicates based on their masses and retention time within a match time window of 0.7 min and using an alignment time window of 20 min. The quantification was performed using a minimum ratio count of 1 (unique + razor) and the second peptide option to allow identification of two cofragmented coeluting peptides with similar masses. The false discovery rate (FDR) at the peptide level and protein level were set to 1% and determined by searching a reverse database. For protein grouping, all proteins that cannot be distinguished based on their identified peptides were assembled into a single entry according to the MaxQuant rules. The statistical analysis was done with Perseus program (version 1.5.1.6) from the MaxQuant environment. The LFQ normalized intensities were uploaded from the proteinGroups.txt file. First, proteins marked as contaminant, reverse hits, and only identified by site were discarded. Quantifiable proteins were defined as those detected in at least 100% of samples in at least one condition. Protein LFQ intensities were base 2 logarithmized to obtain a normal distribution. Missing values were replaced using data imputation by randomly selecting from a normal distribution centered on the lower edge of the intensity values that simulates signals of low abundant proteins using default parameters (a downshift of 1.8 standard deviation and a width of 0.3 of the original distribution). In this way, imputation of missing values in the controls allows statistical comparison of protein abundances that are present only in the immunoprecipitation samples. To determine whether a given detected protein was specifically associated with the bait, we compared the distributions of normalized log intensities between WT and RLTPR^{OST} backgrounds by computing the P-value from a nonparametric Wilcoxon test along with the fold-change. Proteins were selected as specific partners of the bait when both $P < 0.05$ and the corresponding enrichment was greater than threefold. The proteomics data, including search results, have been deposited in the PRIDE repository of the ProteomeXchange Consortium under accession no. PXD003870.

CRISPR-Cas9–based genome editing of Jurkat T cells

sgRNA-specifying oligonucleotide sequences were chosen to minimize the likelihood of off-target cleavage based on publicly available on-line tools (https://www.dna20.com/products). The following pairs of sgRNA-specifying oligonucleotide sequences have been used: *Rltpr*$^{-}$, boundary of 5′ deletion, 5′-*CACCG*GTTTCCCGCCGGAGCTCGT-3′ and 5′-*AAAC*ACGAGCTCCGGCGGGAAAC*C*-3′; *Rltpr*$^{-}$, boundary of 3′ deletion, 5′-*CACCG*CCCTAGGTCACCTTTGAGC-3′ and 5′-*AAAC*GCTCAAAGGTGACCTAGGG*C*-3′; *Rltpr*^{dph}: boundary of 5′ deletion: 5′-*CACCG*GGAGATGCCGTCGGGGGTC-3′ and 5′-*AAAC*GACCCCCGACGGCATCTCC*C*-3′ and boundary of 3′ deletion: 5′-*CACCG*CCCCTATCCCCTCCCCAGG-3′ and 5′*AAAC*CCTGGGGAGGGGATAGGGG*C*-3′, *Rltpr*^{dprr}: boundary of 5′ deletion: 5′-*CACCG*GGGGCCAACAGGATGGTCC-3′ and 5′-*AAAC*GGACCATCCTGTTGGCCCC*C*-3′ and boundary of 3′ deletion: 5′-*CACC*GAGAGGAGAGGATCAGGGAT-3′ and 5′-*AAAC*ATCCCTGATCCTCTCCTCTC-3′; *Rltpr*^{ost}: 5′-*CACC*GAGAGGAGAGGATCAGGGAT-3′ and 5′-*AAAC*ATCCCTGATCCTCTCCTCTC-3′. The guide oligos contained overhangs for ligation into BbsI sites of plasmids pX330 and pX335 and a G-C base pair (italics) was added at the 5′ end of the guide sequence for T7 transcription. The annealed oligonucleotides were cloned into plasmid pX330 (pSpCas9; Addgene plasmid ID 42230) or into plasmid pX335 (hSpCas9n D10A; Addgene

plasmid ID 42335). Double-stranded DNA repair templates (targeting vector) containing the desired edited sequence, as well as additional homologous sequence immediately upstream and downstream (homology arms) of the edited sequence, were assembled. The size of the left and right homology arms of the targeting vector was 500 bp. To prevent CRISPR-Cas9 cleavage of the targeting vectors, a silent mutation destroying the PAM sequence that is present in the genomic DNA was introduced into them. Finally, a *LoxP*-flanked NeoR cassette was introduced in the intron that flanked the exon subjected to edition. Jurkat, Clone E6-1 cells were nucleofected using the Cell Line Nucleofector kit V program I-010 for Nucleofector II with 2.5 µg of linearized targeting vector, and 10 µg pX330-sgRNA or pX335-sgRNA plasmid. Cells were allowed to recover for 48 h, and then subjected to G418 selection (2 mg/ml). Cells growing in G418 were then cloned by limiting dilution and screened for proper gene editing using PCR and genomic DNA sequencing. Transient expression of a Cre recombinase in correctly recombined Jurkat T cell clones allowed for the removal of the floxed Neo^R cassette. Therefore, in addition to the intended mutation, each mutated allele contains a LoxP site in the 5′ or 3′ intron flanking the exon harboring the intended mutation. Clones with monoallelic mutation were defined as having PCR amplification of both the WT and mutated bands. Clones with biallelic mutation were defined as having PCR amplification of the mutated band and absence of the WT band. If a biallelic mutation was not obtained after a single round of nucleofection, clones lacking insertion-deletion (indel) in the untouched allele were subjected first to transient Cre expression to remove the Neo^R cassette present in the properly targeted allele, and then to a second round of nucleofection using the same targeting vector and pX330-sgRNA plasmid.

Jurkat T cell stimulation

The human leukemic T cell line Jurkat and Raji lymphoblastoid B cell line were provided by A. Weiss (University of California, San Francisco, San Francisco, CA). Jurkat T cells (10^5) were stimulated by co-culture with Raji cells (0.5×10^5) presenting the superantigen SEE (Toxin Technology), which binds to both the TCR and MHC class II molecules. IL-2 production by Jurkat cells 24 h after stimulation with Raji and SEE was measured by ELISA (R&D Systems).

Lentiviral infection of Jurkat T cells

cDNA coding for WT and mutant forms of RLTPR were cloned into the CD550A-1 lentiviral vector and RLTPR-deficient Jurkat cells retroinfected with a LentiStarter kit 2.0 (System Biosciences). Infected Jurkat cells were cloned and selected for expressing levels of CD3, CD28, and RLTPR comparable to WT Jurkat cells.

Biochemistry

Immunoblot analysis was performed as previously described (Roncagalli et al., 2014). Antibodies to ERK1-2 (9102), phospho-T202/Y204-ERK1/2 (9106), anti-GFP (2555), and SLP76 (4958) were obtained from Cell Signaling Technology, and the anti–CAPZA-1 (AB6016) was purchased from Millipore.

Expression in HEK293 cells

cDNA coding for $RLTPR^{OST}$ and $RLTPR^{YPET}$ were inserted into pMx-IRES-EFGP (Mingueneau et al., 2009) and transfected into HEK293 using Lipofectamine 2000 (Thermo Fisher Scientific). After 48 h, cells were lysed and equivalent amount of proteins were incubated with Strep-Tactin Sepharose beads for 1.5 h at 4°C on a rotary wheel. Beads were then washed and protein complexes were eluted with 2.5 mM D-biotin and analyzed by immunoblot as specified.

In vitro Th differentiation of $CD4^+$ T cells

Sorted naive $CD4^+$ T cells (2×10^5) were stimulated for 5 d with plate-bound anti-CD3 (3 µg/ml) and soluble anti-CD28 (1 µg/ml) under Th1 (10 µg/ml anti–IL-4 antibodies, 5 U/ml IL-2, and 10 ng/ml IL-12), Th2 (10 µg/ml anti–IFN-γ antibodies, 50 ng/ml IL-4, and 5 U/ml IL-2) or Th17 (10 µg/ml anti–IFN-γ antibodies, 5 µg/ml anti–IL-4 antibodies, 50 ng/ml IL-6, 1 ng/ml TGF-β, and 5 ng/ml IL-23) differentiating conditions. Cultures were split on day 3 and re-fed with Th differentiation cocktail. After 5 d of culture, cells were further incubated for 4 h in the presence of PMA (5 ng/ml), ionomycin (250 ng/ml), and monensin (Golgistop; BD). Cells were stained for extracellular markers and then permeabilized with a Cytofix/Cytoperm kit (BD). Intracellular cytokines were detected using anti IFN-γ (XMG1.2), anti–IL-4 (11B11), and anti–IL-17 (559502) antibodies.

B cell responses

To evaluate T cell–independent B cell responses, mice of the specified genotype (four per group) were immunized with 20 µg of TNP-LPS (Biosearch Technologies) in 100 µl of PBS. Mice were bled before and 7 d after immunization. To evaluate T cell–dependent B cell responses, mice of the specified genotype (four per group) were immunized intraperitoneally with 100 µg of TNP-KLH (Biosearch Technologies) emulsified in complete Freund adjuvant at day 0 and 14. Mice were bled before and 21 d after immunization. Serum antibodies specific for TNP were measured at the specified time points using plates coated with TNP-BSA (10 µg/ml). Plates incubated with serial sample dilutions were developed with isotype-specific antibodies (SBA Clonotyping System/HRP; Southern Biotech), and the concentration of bound antibodies was determined using IgM, IgG2a, IgG2b, and IgG1 isotype standards.

Proliferative responses of splenic B cells

B cells were purified from the spleen using a Dynabeads Untouched B cells kit (Thermo Fisher Scientific) and cultured (10^5 cells in 100 µl of medium). B cells were stimulated with graded doses of $F(ab)'_2$ goat anti–mouse IgM antibody (Jackson ImmunoResearch Laboratories), anti-CD40 (FGK45.5; 1 µg/ml) antibody, or LPS (1 µg/ml). After 4 d

of culture, B cell proliferation was evaluated by addition of 100 µl of CellTiter-Glo reagent (Promega).

CD28 internalization assay

Cells were incubated for 30 min on ice with anti-CD28 (1 µg/ml; 553294; BD), followed by incubation for another 30 min on ice with biotinylated goat antibody to hamster immunoglobulin G (2 µg/ml; 107–066-142; Jackson ImmunoResearch Laboratories). Cells were then washed and warmed to 37°C for 5, 10, or 15 min to allow internalization, and then treated with 0.1% NaN3 on ice. Cells were stained with phycoerythrin-conjugated streptavidin, washed, and analyzed by flow cytometry.

Online supplemental material

Fig. S1 shows the generation and validation of knock-in mice expressing endogenous RLTPR proteins tagged with a One-STrEP-tag (OST) sequence. Fig. S2 assesses the biological and technical variability across samples. Fig. S3 shows the generation and validation of RLTPR-deficient mice. Fig. S4 shows the generation and validation of *Rltpr*^{dcpi} mice. Table S1 (available as an Excel file) shows the list of proteins associated with RLTPR in resting thymocytes and in thymocytes stimulated with pervanadate for 30, 120, 300, and 600 s.

ACKNOWLEDGMENTS

We thank Jean-Laurent Casanova, Vivien Beziat, Guillaume Voisinne, Adam Zwolak, Elena Tomasello, and John Hammer for discussion; Arthur Weiss for providing the Jurkat cell line; and Ingrid Hinchliffe and Fabien Angelis for construction of the mice.

This work was supported by Centre National de la Recherche Scientifique, Institut National de la Santé et de la Recherche Médicale, European Research Council (ERC; FP7/2007–2013 grant no. 322465 [Integrate] to B. Malissen), Agence Nationale de la Recherche (Basilic project to M. Malissen), PHENOMIN, and fellowships from the Axa Research Fund (M. Cucchetti) and the ERC grant Integrate (M. Cucchetti, M.G. Menoita, and S. Durand). The anti-RLTPR antibody has been developed in the frame of the Sybilla European Integrating Project. Proteomics analysis was performed by the Marseille Proteomics facility supported by Infrastructures Biologie Santé et Agronomie, Cancéropôle PACA, the Provence-Alpes-Côte d'Azur Region, Institut Paoli-Calmettes, Centre de Recherche en Cancérologie de Marseille, and Provence-Alpes-Côte d'Azur Region.

The authors declare no competing financial interests.

Author contributions: B. Malissen, M. Malissen, and R. Roncagalli conceived the project; B. Malissen and F. Fiore designed the *Rltpr*^{ost}, *Rltpr*^{dcpi}, and *Rltpr*$^{-}$ mice; M. Malissen, E. Bergot, Y. Liang, and R. Roncagalli analyzed the phenotype of mutant mice; R. Roncagalli, M. Goncalves Menoita, and S. Durand performed biochemical experiments; R. Roncagalli and M. Cucchetti analyzed Jurkat T cells; M. Cucchetti, B. Malissen, and M. Suchanek generated the EM-53 antibody and characterized its specificity; M. Cucchetti, M. Cucchetti, C. Grégoire, and L. Zhang performed CRISPR-Cas9 gene editing; S. Audebert, E. Baudelet, and L. Camoin performed the MS experiments; A. Joachim and M. Malissen analyzed B cells and pDC; and B. Malissen, M. Malissen, and R. Roncagalli wrote the manuscript.

Submitted: 22 April 2016
Accepted: 17 August 2016

REFERENCES

Ai, H.W., J.N. Henderson, S.J. Remington, and R.E. Campbell. 2006. Directed evolution of a monomeric, bright and photostable version of Clavularia cyan fluorescent protein: structural characterization and applications in fluorescence imaging. *Biochem. J.* 400:531–540. http://dx.doi.org/10.1042/BJ20060874

Bunting, M., K.E. Bernstein, J.M. Greer, M.R. Capecchi, and K.R. Thomas. 1999. Targeting genes for self-excision in the germ line. *Genes Dev.* 13:1524–1528. http://dx.doi.org/10.1101/gad.13.12.1524

Chiossone, L., J. Chaix, N. Fuseri, C. Roth, E. Vivier, and T. Walzer. 2009. Maturation of mouse NK cells is a 4-stage developmental program. *Blood.* 113:5488–5496. http://dx.doi.org/10.1182/blood-2008-10-187179

Cox, J., and M. Mann. 2008. MaxQuant enables high peptide identification rates, individualized p.p.b.-range mass accuracies and proteome-wide protein quantification. *Nat. Biotechnol.* 26:1367–1372. http://dx.doi.org/10.1038/nbt.1511

Cox, J., N. Neuhauser, A. Michalski, R.A. Scheltema, J.V. Olsen, and M. Mann. 2011. Andromeda: a peptide search engine integrated into the MaxQuant environment. *J. Proteome Res.* 10:1794–1805. http://dx.doi.org/10.1021/pr101065j

Cox, J., M.Y. Hein, C.A. Luber, I. Paron, N. Nagaraj, and M. Mann. 2014. Accurate proteome-wide label-free quantification by delayed normalization and maximal peptide ratio extraction, termed MaxLFQ. *Mol. Cell. Proteomics.* 13:2513–2526. http://dx.doi.org/10.1074/mcp.M113.031591

Delogu, A., A. Schebesta, Q. Sun, K. Aschenbrenner, T. Perlot, and M. Busslinger. 2006. Gene repression by Pax5 in B cells is essential for blood cell homeostasis and is reversed in plasma cells. *Immunity.* 24:269–281. http://dx.doi.org/10.1016/j.immuni.2006.01.012

Dodson, L.F., J.S. Boomer, C.M. Deppong, D.D. Shah, J. Sim, T.L. Bricker, J.H. Russell, and J.M. Green. 2009. Targeted knock-in mice expressing mutations of CD28 reveal an essential pathway for costimulation. *Mol. Cell. Biol.* 29:3710–3721. http://dx.doi.org/10.1128/MCB.01869-08

Eastburn, D.J., M.M. Zegers, and K.E. Mostov. 2012. Scrib regulates HGF-mediated epithelial morphogenesis and is stabilized by Sgt1-HSP90. *J. Cell Sci.* 125:4147–4157. http://dx.doi.org/10.1242/jcs.108670

Edwards, M., A. Zwolak, D.A. Schafer, D. Sept, R. Dominguez, and J.A. Cooper. 2014. Capping protein regulators fine-tune actin assembly dynamics. *Nat. Rev. Mol. Cell Biol.* 15:677–689. http://dx.doi.org/10.1038/nrm3869

Fan, Q.R., and W.A. Hendrickson. 2005. Structure of human follicle-stimulating hormone in complex with its receptor. *Nature.* 433:269–277. http://dx.doi.org/10.1038/nature03206

Fujiwara, I., K. Remmert, and J.A. Hammer III. 2010. Direct observation of the uncapping of capping protein-capped actin filaments by CARMIL homology domain 3. *J. Biol. Chem.* 285:2707–2720. http://dx.doi.org/10.1074/jbc.M109.031203

Galea-Lauri, J., D. Darling, S.U. Gan, L. Krivochtchapov, M. Kuiper, J. Gäken, B. Souberbielle, and F. Farzaneh. 1999. Expression of a variant of CD28 on a subpopulation of human NK cells: implications for B7-mediated stimulation of NK cells. *J. Immunol.* 163:62–70.

Hernandez-Valladares, M., T. Kim, B. Kannan, A. Tung, A.H. Aguda, M. Larsson, J.A. Cooper, and R.C. Robinson. 2010. Structural characterization of a capping protein interaction motif defines a family of actin filament regulators. *Nat. Struct. Mol. Biol.* 17:497–503. http://dx.doi.org/10.1038/nsmb.1792

Higo, K., M. Oda, H. Morii, J. Takahashi, Y. Harada, S. Ogawa, and R. Abe. 2014. Quantitative analysis by surface plasmon resonance of CD28 interaction with cytoplasmic adaptor molecules Grb2, Gads and p85 PI3K. *Immunol. Invest.* 43:278–291. http://dx.doi.org/10.3109/08820139.2013.875039

Horejsí, V., W. Zhang, and B. Schraven. 2004. Transmembrane adaptor proteins: organizers of immunoreceptor signalling. *Nat. Rev. Immunol.* 4:603–616. http://dx.doi.org/10.1038/nri1414

Hukelmann, J.L., K.E. Anderson, L.V. Sinclair, K.M. Grzes, A.B. Murillo, P.T. Hawkins, L.R. Stephens, A.I. Lamond, and D.A. Cantrell. 2016. The

cytotoxic T cell proteome and its shaping by the kinase mTOR. *Nat. Immunol.* 17:104–112. http://dx.doi.org/10.1038/ni.3314

Jiang, C., and X. Lin. 2012. Regulation of NF-κB by the CARD proteins. *Immunol. Rev.* 246:141–153. http://dx.doi.org/10.1111/j.1600-065X.2012.01110.x

Junttila, M.R., S. Saarinen, T. Schmidt, J. Kast, and J. Westermarck. 2005. Single-step Strep-tag purification for the isolation and identification of protein complexes from mammalian cells. *Proteomics.* 5:1199–1203. http://dx.doi.org/10.1002/pmic.200400991

Kibe, T., G.A. Osawa, C.E. Keegan, and T. de Lange. 2010. Telomere protection by TPP1 is mediated by POT1a and POT1b. *Mol. Cell. Biol.* 30:1059–1066. http://dx.doi.org/10.1128/MCB.01498-09

Kim, T., G.E. Ravilious, D. Sept, and J.A. Cooper. 2012. Mechanism for CARMIL protein inhibition of heterodimeric actin-capping protein. *J. Biol. Chem.* 287:15251–15262. http://dx.doi.org/10.1074/jbc.M112.345447

Kong, K.F., T. Yokosuka, A.J. Canonigo-Balancio, N. Isakov, T. Saito, and A. Altman. 2011. A motif in the V3 domain of the kinase PKC-θ determines its localization in the immunological synapse and functions in T cells via association with CD28. *Nat. Immunol.* 12:1105–1112. http://dx.doi.org/10.1038/ni.2120

Lanier, M.H., T. Kim, J.A. Cooper, E. Judokusumo, G. Carmona, F.B. Gertler, L.C. Kam, C.V. Carman, J.K. Burkhardt, D.J. Irvine, and M.L. Dustin. 2015. CARMIL2 is a novel molecular connection between vimentin and actin essential for cell migration and invadopodia formation. *Mol. Biol. Cell.* 26:4577–4588. http://dx.doi.org/10.1091/mbc.E15-08-0552

Lanier, M.H., P. McConnell, and J.A. Cooper. 2016. Cell migration and invadopodia formation require a membrane-binding domain of CARMIL2. *J. Biol. Chem.* 291:1076–1091. http://dx.doi.org/10.1074/jbc.M115.676882

Liang, Y., H. Niederstrasser, M. Edwards, C.E. Jackson, and J.A. Cooper. 2009. Distinct roles for CARMIL isoforms in cell migration. *Mol. Biol. Cell.* 20:5290–5305. http://dx.doi.org/10.1091/mbc.E08-10-1071

Liang, Y., M. Cucchetti, R. Roncagalli, T. Yokosuka, A. Malzac, E. Bertosio, J. Imbert, I.J. Nijman, M. Suchanek, T. Saito, et al. 2013. The lymphoid lineage-specific actin-uncapping protein Rltpr is essential for costimulation via CD28 and the development of regulatory T cells. *Nat. Immunol.* 14:858–866. http://dx.doi.org/10.1038/ni.2634

Macal, M., M.A. Tam, C. Hesser, J. Di Domizio, P. Leger, M. Gilliet, and E.I. Zuniga. 2016. CD28 Deficiency Enhances Type I IFN production by murine plasmacytoid dendritic cells. *J. Immunol.* 196:1900–1909. http://dx.doi.org/10.4049/jimmunol.1501658

Malissen, B., C. Grégoire, M. Malissen, and R. Roncagalli. 2014. Integrative biology of T cell activation. *Nat. Immunol.* 15:790–797. http://dx.doi.org/10.1038/ni.2959

Marinari, B., A. Costanzo, A. Viola, F. Michel, G. Mangino, O. Acuto, M. Levrero, E. Piccolella, and L. Tuosto. 2002. Vav cooperates with CD28 to induce NF-kappaB activation via a pathway involving Rac-1 and mitogen-activated kinase kinase 1. *Eur. J. Immunol.* 32:447–456. http://dx.doi.org/10.1002/1521-4141(200202)32:2<447::AID-IMMU447>3.0.CO;2-5

Mingueneau, M., R. Roncagalli, C. Grégoire, A. Kissenpfennig, A. Miazek, C. Archambaud, Y. Wang, P. Perrin, E. Bertosio, A. Sansoni, et al. 2009. Loss of the LAT adaptor converts antigen-responsive T cells into pathogenic effectors that function independently of the T cell receptor. *Immunity.* 31:197–208. http://dx.doi.org/10.1016/j.immuni.2009.05.013

Okkenhaug, K., L. Wu, K.M. Garza, J. La Rose, W. Khoo, B. Odermatt, T.W. Mak, P.S. Ohashi, and R. Rottapel. 2001. A point mutation in CD28 distinguishes proliferative signals from survival signals. *Nat. Immunol.* 2:325–332. http://dx.doi.org/10.1038/86327

Pagán, A.J., M. Pepper, H.H. Chu, J.M. Green, and M.K. Jenkins. 2012. CD28 promotes CD4+ T cell clonal expansion during infection independently of its YMNM and PYAP motifs. *J. Immunol.* 189:2909–2917. http://dx.doi.org/10.4049/jimmunol.1103231

Pettitt, S.J., Q. Liang, X.Y. Rairdan, J.L. Moran, H.M. Prosser, D.R. Beier, K.C. Lloyd, A. Bradley, and W.C. Skarnes. 2009. Agouti C57BL/6N embryonic stem cells for mouse genetic resources. *Nat. Methods.* 6:493–495. http://dx.doi.org/10.1038/nmeth.1342

Raab, M., S. Pfister, and C.E. Rudd. 2001. CD28 signaling via VAV/SLP-76 adaptors: regulation of cytokine transcription independent of TCR ligation. *Immunity.* 15:921–933. http://dx.doi.org/10.1016/S1074-7613(01)00248-5

Rodríguez, C.I., F. Buchholz, J. Galloway, R. Sequerra, J. Kasper, R. Ayala, A.F. Stewart, and S.M. Dymecki. 2000. High-efficiency deleter mice show that FLPe is an alternative to Cre-loxP. *Nat. Genet.* 25:139–140. http://dx.doi.org/10.1038/75973

Roncagalli, R., S. Hauri, F. Fiore, Y. Liang, Z. Chen, A. Sansoni, K. Kanduri, R. Joly, A. Malzac, H. Lähdesmäki, et al. 2014. Quantitative proteomics analysis of signalosome dynamics in primary T cells identifies the surface receptor CD6 as a Lat adaptor-independent TCR signaling hub. *Nat. Immunol.* 15:384–392. http://dx.doi.org/10.1038/ni.2843

Rozanski, C.H., A. Utley, L.M. Carlson, M.R. Farren, M. Murray, L.M. Russell, J.R. Nair, Z. Yang, W. Brady, L.A. Garrett-Sinha, et al. 2015. CD28 promotes plasma cell survival, sustained antibody responses, and BLIMP-1 upregulation through its distal PYAP proline motif. *J. Immunol.* 194:4717–4728. http://dx.doi.org/10.4049/jimmunol.1402260

Shahinian, A., K. Pfeffer, K.P. Lee, T.M. Kündig, K. Kishihara, A. Wakeham, K. Kawai, P.S. Ohashi, C.B. Thompson, and T.W. Mak. 1993. Differential T cell costimulatory requirements in CD28-deficient mice. *Science.* 261:609–612. http://dx.doi.org/10.1126/science.7688139

Shevchenko, A., M. Wilm, O. Vorm, and M. Mann. 1996. Mass spectrometric sequencing of proteins silver-stained polyacrylamide gels. *Anal. Chem.* 68:850–858. http://dx.doi.org/10.1021/ac950914h

Shirasu, K. 2009. The HSP90-SGT1 chaperone complex for NLR immune sensors. *Annu. Rev. Plant Biol.* 60:139–164. http://dx.doi.org/10.1146/annurev.arplant.59.032607.092906

Soriano, P. 1997. The PDGF alpha receptor is required for neural crest cell development and for normal patterning of the somites. *Development.* 124:2691–2700.

Soskic, B., O.S. Qureshi, T. Hou, and D.M. Sansom. 2014. A transendocytosis perspective on the CD28/CTLA-4 pathway. *Adv. Immunol.* 124:95–136. http://dx.doi.org/10.1016/B978-0-12-800147-9.00004-2

Srivastava, R., B.J. Burbach, and Y. Shimizu. 2010. NF-kappaB activation in T cells requires discrete control of IkappaB kinase alpha/beta (IKKalpha/beta) phosphorylation and IKKgamma ubiquitination by the ADAP adapter protein. *J. Biol. Chem.* 285:11100–11105. http://dx.doi.org/10.1074/jbc.M109.068999

Tan, Y.X., B.N. Manz, T.S. Freedman, C. Zhang, K.M. Shokat, and A. Weiss. 2014. Inhibition of the kinase Csk in thymocytes reveals a requirement for actin remodeling in the initiation of full TCR signaling. *Nat. Immunol.* 15:186–194. http://dx.doi.org/10.1038/ni.2772

Thome, M., J.E. Charton, C. Pelzer, and S. Hailfinger. 2010. Antigen receptor signaling to NF-kappaB via CARMA1, BCL10, and MALT1. *Cold Spring Harb. Perspect. Biol.* 2:a003004. http://dx.doi.org/10.1101/cshperspect.a003004

Tian, R., H. Wang, G.D. Gish, E. Petsalaki, A. Pasculescu, Y. Shi, M. Mollenauer, R.D. Bagshaw, N. Yosef, T. Hunter, et al. 2015. Combinatorial proteomic analysis of intercellular signaling applied to the CD28 T-cell costimulatory receptor. *Proc. Natl. Acad. Sci. USA.* 112:E1594–E1603. http://dx.doi.org/10.1073/pnas.1503286112

Vang, K.B., J. Yang, A.J. Pagán, L.X. Li, J. Wang, J.M. Green, A.A. Beg, and M.A. Farrar. 2010. Cutting edge: CD28 and c-Rel-dependent pathways initiate regulatory T cell development. *J. Immunol.* 184:4074–4077. http://dx.doi.org/10.4049/jimmunol.0903933

Wang, X., H.C. Chuang, J.P. Li, and T.H. Tan. 2012. Regulation of PKC-θ function by phosphorylation in T cell receptor signaling. *Front. Immunol.* 3:197. http://dx.doi.org/10.3389/fimmu.2012.00197

Wang, Y., C.S. Ma, Y. Ling, A. Bousfiha, Y. Camcioglu, S. Jacquot, K. Payne, E. Crestani, R. Roncagalli, A. Belkadi, et al.. 2016. Dual T cell– and B cell–intrinsic deficiency in humans with biallelic RLTPR mutations. *J. Exp. Med*. This issue. http://dx.doi.org/10.1084/jem.20160576

Yang, C., M. Pring, M.A. Wear, M. Huang, J.A. Cooper, T.M. Svitkina, and S.H. Zigmond. 2005. Mammalian CARMIL inhibits actin filament capping by capping protein. *Dev. Cell*. 9:209–221. http://dx.doi.org/10.1016/j.devcel.2005.06.008

Yokosuka, T., and T. Saito. 2010. The immunological synapse, TCR microclusters, and T cell activation. *Curr. Top. Microbiol. Immunol.* 340:81–107. http://dx.doi.org/10.1007/978-3-642-03858-7_5

Zhang, Q., C.G. Dove, J.L. Hor, H.M. Murdock, D.M. Strauss-Albee, J.A. Garcia, J.N. Mandl, R.A. Grodick, H. Jing, D.B. Chandler-Brown, et al. 2014. DOCK8 regulates lymphocyte shape integrity for skin antiviral immunity. *J. Exp. Med*. 211:2549–2566. http://dx.doi.org/10.1084/jem.20141307

Zhang, Y., J.P. Muyrers, G. Testa, and A.F. Stewart. 2000. DNA cloning by homologous recombination in Escherichia coli. *Nat. Biotechnol.* 18:1314–1317. http://dx.doi.org/10.1038/82449

Zwolak, A., C. Yang, E.A. Feeser, E.M. Ostap, T. Svitkina, and R. Dominguez. 2013. CARMIL leading edge localization depends on a non-canonical PH domain and dimerization. *Nat. Commun*. 4:2523. http://dx.doi.org/10.1038/ncomms3523